

Quantifying net community production and calcification at Station ALOHA near Hawai'i: Insights and limitations from a dual tracer carbon budget approach

Lucie Anna Christa Maria Knor¹, Christopher L. Sabine², Adrienne J. Sutton³, John E. Dore⁴, Angelique E. White¹, James Potemra¹, and Robert A. Weller⁵

¹University of Hawaii at Manoa

²University of Hawaii Manoa

³NOAA Pacific Marine Environmental Laboratory

⁴Montana State University, US

⁵Woods Hole Oceanographic Institution

December 13, 2022

Abstract

A budget approach is used to disentangle drivers of the seasonal mixed layer carbon cycle at Station ALOHA (A Long-term Oligotrophic Habitat Assessment) in the North Pacific Subtropical Gyre (NPSG). The budget utilizes data from the WHOTS (Woods Hole - Hawaii Ocean Time-series Site) mooring, and the ship-based Hawai'i Ocean Time-series (HOT) in the North Pacific Subtropical Gyre (NPSG), a region of significant oceanic carbon uptake. Parsing the carbon variations into process components allows an assessment of both the proportional contributions of mixed layer carbon drivers, and the seasonal interplay of drawdown and supply from different processes. Annual net community production reported here is at the lower end of previously published data, while net community calcification estimates are 4- to 7-fold higher than available sediment trap data, the only other estimate of calcium carbonate export at this location. Although the observed seasonal cycle in dissolved inorganic carbon (DIC) in the NPSG has a relatively small amplitude, larger fluxes offset each other over an average year, with major supply from physical transport, especially lateral eddy transport throughout the year and entrainment in the winter, and biological carbon uptake in the spring. Gas exchange plays a smaller role, supplying carbon to the surface ocean between Dec-May, and outgassing in Jul-Oct. Evaporation-precipitation (E-P) is variable with precipitation prevailing in the first- and evaporation in the second half of the year. The observed total alkalinity signal is largely governed by E-P, with a somewhat stronger net calcification signal in the wintertime.

Hosted file

951939_0_art_file_10526779_rmrcvc.docx available at <https://authorea.com/users/565835/articles/612710-quantifying-net-community-production-and-calcification-at-station-aloha-near-hawai-i-insights-and-limitations-from-a-dual-tracer-carbon-budget-approach>

Hosted file

951939_0_supp_10526780_rmqn01.docx available at <https://authorea.com/users/565835/articles/612710-quantifying-net-community-production-and-calcification-at-station-aloha-near-hawai-i-insights-and-limitations-from-a-dual-tracer-carbon-budget-approach>

Hosted file

951939_0_video_10526782_rmqn02.gif available at <https://authorea.com/users/565835/articles/612710-quantifying-net-community-production-and-calcification-at-station-aloha-near-hawai-i-insights-and-limitations-from-a-dual-tracer-carbon-budget-approach>

Hosted file

951939_0_video_10526783_rmqn02.gif available at <https://authorea.com/users/565835/articles/612710-quantifying-net-community-production-and-calcification-at-station-aloha-near-hawai-i-insights-and-limitations-from-a-dual-tracer-carbon-budget-approach>

1
2
3
4
5
6
7
8
9
10
11
12
13
14
15
16
17

Quantifying net community production and calcification at Station ALOHA near Hawai'i: Insights and limitations from a dual tracer carbon budget approach

**Lucie A. C. M. Knor¹, Christopher L. Sabine¹, Adrienne J. Sutton², John Dore³,
Angelicque E. White¹, James Potemra¹, and Robert A. Weller⁴**

¹University of Hawai'i at Mānoa, Honolulu, Hawai'i, USA

²NOAA Pacific Marine Environmental Laboratory, Seattle, Washington, USA

³Montana State University, Bozeman, Montana, USA

⁴Woods Hole Oceanographic Institution, Falmouth, Massachusetts, USA

Corresponding author: Lucie Anna Christa Maria Knor (luciek@hawaii.edu)

Key Points:

- First calculation of community calcification with a budget approach at this location, results exceed reported sediment trap data.
- Calculated net community production confirms net autotrophy over a year, on the lower end of previous estimates.
- It is important to better constrain physical, especially horizontal, transport of carbon to further investigate mixed layer carbon cycling.

18 Abstract

19 A budget approach is used to disentangle drivers of the seasonal mixed layer carbon cycle
20 at Station ALOHA (A Long-term Oligotrophic Habitat Assessment) in the North Pacific
21 Subtropical Gyre (NPSG). The budget utilizes data from the WHOTS (Woods Hole - Hawaii
22 Ocean Time-series Site) mooring, and the ship-based Hawai'i Ocean Time-series (HOT) in the
23 North Pacific Subtropical Gyre (NPSG), a region of significant oceanic carbon uptake. Parsing
24 the carbon variations into process components allows an assessment of both the proportional
25 contributions of mixed layer carbon drivers, and the seasonal interplay of drawdown and supply
26 from different processes. Annual net community production reported here is at the lower end of
27 previously published data, while net community calcification estimates are 4- to 7-fold higher
28 than available sediment trap data, the only other estimate of calcium carbonate export at this
29 location. Although the observed seasonal cycle in dissolved inorganic carbon (DIC) in the NPSG
30 has a relatively small amplitude, larger fluxes offset each other over an average year, with major
31 supply from physical transport, especially lateral eddy transport throughout the year and
32 entrainment in the winter, and biological carbon uptake in the spring. Gas exchange plays a
33 smaller role, supplying carbon to the surface ocean between Dec-May, and outgassing in Jul-Oct.
34 Evaporation-precipitation (E-P) is variable with precipitation prevailing in the first- and
35 evaporation in the second half of the year. The observed total alkalinity signal is largely
36 governed by E-P, with a somewhat stronger net calcification signal in the wintertime.

37 Plain Language Summary

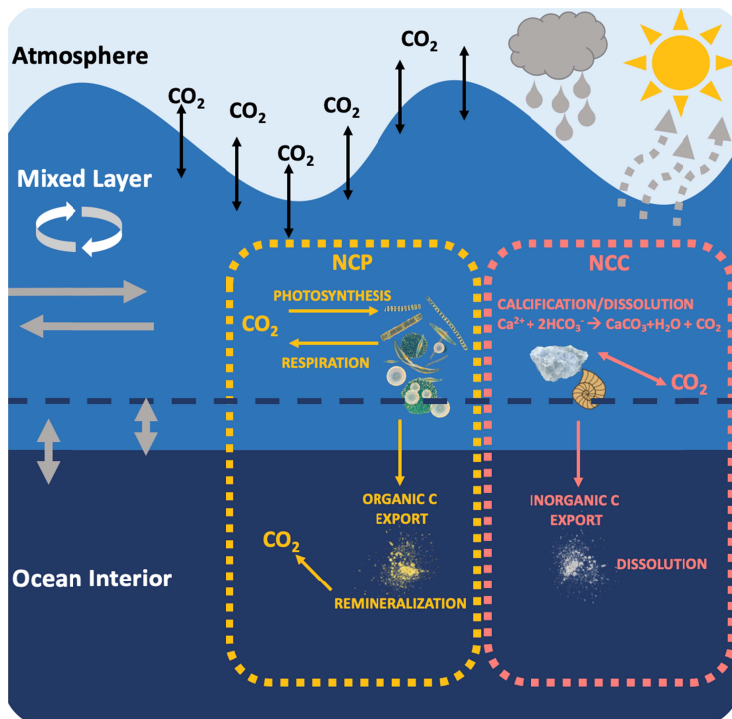
38 The ocean carbon cycle is a complicated system. In it, chemical compounds react, are moved by
39 ocean physics, altered by organisms, and exchange with CO₂ in the atmosphere. To explore how
40 the ocean will continue to take up CO₂ from the atmosphere, and how much will be removed into
41 the deep ocean, we need to know how these processes influence ocean carbon. Here, we
42 investigate them over a year. We create a model from observations of two carbon compounds,
43 together with calculated estimates of processes (evaporation and precipitation, transport through
44 the water, and air-sea exchange) to back out the influence of two important reaction pairs
45 executed by organisms: Photosynthesis and respiration, and calcification and dissolution. Over a
46 year, the surface community at this location near Hawai'i in the Pacific photosynthesizes more
47 than it respire, removing 66 grams of CO₂ per square meter. Also, marine calcifiers perform
48 calcification, and our estimates are much higher than previous measurements from sediment
49 traps. Gas exchange and evaporation-precipitation vary with the seasons in opposite directions,
50 and there are carbon inputs from horizontal transport throughout the year, and from water
51 column mixing in the winter.

52

53 1 Introduction

54 1.1 Rationale

55 The biological pumps are a fundamental component of the global carbon cycle, driving the
 56 transfer of carbon from the atmosphere to the deep ocean. Multiple surface ocean processes
 57 play a role in carbon concentrations and export from the mixed layer, including physical (gas
 58 exchange, evaporation and precipitation, advection, vertical mixing) and biogeochemical
 59 processes, namely photosynthesis, respiration, calcification, and dissolution (Figure 1).
 60 Impacts on biological pumps of changing ocean conditions, such as warming, increased
 61 stratification, or ocean acidification due to climate change, could significantly alter marine
 62 carbon cycling, as well as removal and sequestration of atmospheric CO₂ through various
 63 (potential) feedback loops. This includes the potential for shifts in community structure as
 64 ecosystems respond to changing chemistry, enhanced recycling in a warmer surface ocean, or
 65 reduced particle ballasting and calcification, which all impact carbon export (Sabine &
 66 Tanhua, 2010). Consequently, we need to quantify changes in the mixed layer carbon
 67 inventory, both to understand natural variability at different locations, and to identify changes
 68 over time.



69

70 *Figure 1. Schematic of processes driving mixed layer carbon cycling. Processes influencing*
 71 *the organic component/net community production (photosynthesis and respiration, yellow)*
 72 *and inorganic component/calcification (calcification and dissolution, pink) of the biological*
 73 *carbon pump, as well as physical processes (gas exchange, black arrows; evaporation and*
 74 *precipitation, advection, entrainment/detrainment, diffusion, grey arrows).*

75 The North Pacific Subtropical Gyre (NPSG) is an essential system to study when looking at
 76 global carbon cycling. Spanning an area of 2×10^7 km², the NPSG is the largest ecosystem on
 77 earth, and a substantial sink for atmospheric CO₂ (Emerson, 2014). Through the Hawai'i
 78 Ocean Time-series (HOT) at Station ALOHA (A Long-term Oligotrophic Habitat

79 Assessment), one of the longest running oceanic time-series at >30 years, the considerable
80 complexity of this oligotrophic “ocean desert” has been and continues to be investigated,
81 with a focus on biogeochemical cycling of carbon and nutrients, from various angles.
82 Identifying and quantifying the processes at work in the subtropical oligotrophic gyres is
83 difficult due to the very low signal-to-noise ratio in inorganic carbon and associated
84 parameters, and the episodic nature and patchiness of biological variability (Church et al.,
85 2013). Well-constrained community production and calcification would provide an important
86 puzzle piece for understanding current and future ocean regimes in this important ecosystem.

87 Using total alkalinity (TA) and dissolved inorganic carbon (DIC) as tracers, a mass balance
88 of mixed layer carbon production is constructed at Station ALOHA. Both the organic (Net
89 Community Production, NCP) and inorganic (Net Community Calcification, NCC)
90 components of the biological pump are quantified based on the differing stoichiometry of the
91 reactions of interest (Fassbender et al., 2016, 2017). This allows the evaluation of seasonal
92 and interannual variability in drivers of carbon cycling in the NPSG. Thanks to the
93 abundance of complementary and redundant datasets at this well-studied location, multiple
94 approaches to quantify several of the mass balance terms can be evaluated for consistency.
95 Sensitivity analyses of physical transport terms, evaporation and precipitation, and mixed
96 layer definition can illuminate the limitations of an upper ocean carbon budget at this
97 location with present data resolution in space and time.

98 1.2 Study area: Station ALOHA

99 Station ALOHA is a time-series study site with a sampling radius of 9.66 km (6 nm) at
100 22°45'N, 158°W in the NPSG, 100km north of O‘ahu, Hawai‘i. Since 1988, approximately
101 monthly cruises to Station ALOHA have been executed by the Hawai‘i Ocean Time-series
102 (HOT) program, capturing a variety of oceanographic parameters including thermohaline
103 structure, water column chemistry, primary production, plankton community structure,
104 particle export, and currents throughout the water column. In addition, since 2004, moorings
105 within Station ALOHA (2004-2007: MOSEAN Hale-Aloha
106 [www.pmel.noaa.gov/co2/story/HALE-ALOHA] and since 2007: WHOTS
107 [www.soest.hawaii.edu/whots/;

108 www.pmel.noaa.gov/co2/story/WHOTS]) have been recording higher-frequency variability
109 of atmospheric and surface ocean pCO₂ (3-hourly), meteorological data, surface and sub-
110 surface currents (from an Acoustic Doppler current profiler (ADCP) and vector measuring
111 current meters (VMCM, Weller & Davis (1980)), and temperature and salinity in the upper
112 155 m (from conductivity, temperature, depth sensors (CTDs)). The unique combination and
113 extent of observations at this site have enabled multiple ground-breaking discoveries in
114 oceanography, such as the ubiquity of marine archaea, and also including the identification of
115 important patterns influencing carbon biogeochemical cycling (Karl & Church, 2018). The
116 Hawai‘i Ocean Time-series is one of the places where the decrease in surface ocean pH due
117 to anthropogenic CO₂ emissions was first clearly documented. Many researchers have
118 conducted studies on the carbon cycle at Station ALOHA, mainly in the 1990s and early
119 2000s (e.g., Dore et al., 2003, 2009; Keeling et al., 2004; Brix et al., 2004, 2006; Quay &
120 Stutsman, 2003; Neuer et al., 2002; Letelier et al., 2000; Karl et al., 1996; Winn et al., 1994,
121 1998). These studies on biology, physics, and especially the CO₂-carbonate system, carbon
122 cycling, and biological production at this location provide the groundwork for this study.

123 1.3 The ecosystem and carbon cycle at Station ALOHA

124 The ocean in the NPSG is persistently oligotrophic throughout the year with a warm,
125 nutrient-depleted surface layer that is largely isolated from the nutrient-rich deeper waters
126 year-round. Seasons referred to here are defined as spring (March-May), summer (June-
127 August), fall (September-November) and winter (December-February). Most biogeochemical
128 parameters show little seasonality compared to both more temperate environments and other
129 modes of variability (e.g., Karl & Church, 2017; Church et al., 2013). The sea surface
130 temperature only varies by about 4-5°C seasonally (e.g., Brix et al., 2004). The mixed layer
131 is relatively shallow year-round, between 20-120 m (Karl & Lukas, 1996), and the average
132 mixed layer depth changes between \approx 30-40 m in the summer-fall and \approx 70-90 m in the
133 winter. An important component of seasonal variability is the presence of cyclones and
134 associated cold fronts in the winter, which result in strong winds and temporary deepening of
135 the mixed layer (Karl, 1999). The mixed layer only reaches the top of the deep nutricline in
136 late winter to early spring (Ascani et al., 2013). Due to minimal nutrient input, a microbial
137 regeneration loop prevails, where nutrients are largely recycled within the surface layer (Brix
138 et al., 2006). Nitrogen fixation is most variable during the late summer, and generally
139 supplies around 27-45% of particulate nitrogen export (Böttjer et al., 2017). Larger particle
140 export pulses between July-August are supported by diatom-diazotroph assemblages
141 (DDAs), driven by a competitive transition from DDAs in the early summer to other
142 diazotrophs (Follett et al., 2018).

143 Part of the declared goals of the Hawaii Ocean Time-series are to explore “1) *The linkages*
144 *between seasonal, interannual and long-term (...) variability and trends in ocean physics,*
145 *chemistry, and biology. 2) Processes underlying physical and biogeochemical temporal*
146 *variability. 3) The role of physical forcing on carbon fluxes, including rates of biologically*
147 *mediated carbon transformations, air-sea CO₂ exchange, and carbon export.”* (Church et al.,
148 2013). A great deal of effort has already gone into research projects tackling these
149 relationships, but many questions remain unanswered. For example, there is a disagreement
150 in values of NCP from *in situ* compared to *in vitro* methodologies, discussed in detail by
151 Duarte et al. (2013), Ducklow & Doney (2013), and Williams et al. (2013). Additionally,
152 discrepancies between satellite estimates and sediment trap data, which both underestimate
153 NCP compared to mass balance calculations such as the present budget, have been
154 established and addressed, for example, by Emerson (2014). One of the main difficulties in
155 resolving annual net community production and carbon export with upper ocean mass
156 balance calculations has been the inability to fully constrain relevant lateral and vertical
157 transport terms (Keeling et al., 2004; Dore et al., 2003). To complement previous estimates
158 of NCP from other authors using various methodologies, this study aims to independently
159 constrain all physical transport components, thanks to available high temporal resolution data
160 from the WHOTS mooring, as well as horizontal gradient climatologies from neural
161 networks (Sutton et al., 2014, Broullón et al., 2019, 2020). Additionally, a seasonal view of
162 net community calcification is provided for the first time at this location.

163 **2 Data and Methods**

164 2.1 Budget components

165 This carbon budget quantifies a seasonal climatology from a time-dependent monthly mass
 166 balance of carbon (DIC and TA in $\mu\text{mol kg}^{-1}$), integrated over the mixed layer. It is based on
 167 a methodology developed by Fassbender and colleagues (Fassbender et al., 2016, 2017). DIC
 168 and TA are used as dual tracers.

$$(1) \quad \frac{\partial DIC}{\partial t} = \frac{\partial DIC}{\partial t} \Big|_{GasEx} + \frac{\partial DIC}{\partial t} \Big|_{Phys} + \frac{\partial DIC}{\partial t} \Big|_{Evap,Precip} + \frac{\partial DIC}{\partial t} \Big|_{Bio}$$

$$(2) \quad \frac{\partial TA}{\partial t} = \frac{\partial TA}{\partial t} \Big|_{Phys} + \frac{\partial TA}{\partial t} \Big|_{Evap,Precip} + \frac{\partial TA}{\partial t} \Big|_{Bio}$$

169 The observed changes in DIC and TA can be decomposed into individual process
 170 components that are calculated independently: physical transport, evaporation and
 171 precipitation, and, for DIC, gas exchange (Equations 1-2). With all of the process
 172 components and the observed change constrained, the change due to biological processes
 173 is determined from the residual. To examine the seasonal changes, monthly averages are
 174 used for each term. Monthly averages of the variables are computed for months with
 175 >20% data coverage. The physical components of change in DIC and TA over time (gas
 176 exchange, evaporation and precipitation (via concentration and dilution of carbon
 177 species), horizontal and vertical physical transport) are then evaluated and integrated over
 178 the mixed layer.

179 Finally, the biological term is separated into organic (NCP) and inorganic (NCC)
 180 components of biological carbon production, based on stoichiometric ratios from
 181 Anderson & Sarmiento (1994). Because organic matter- and calcium carbonate
 182 production have different effects on DIC vs. TA, we have four equations and four
 183 unknowns and can rearrange to explicitly solve for the changes due to NCP and NCC
 184 (Equations 3-6). A derivation of these equations can be found in the Supplemental
 185 Information of Fassbender et al. (2017). Many of the inputs required for the budget terms
 186 are only available as seasonal climatologies, so the results represent average annual
 187 cycles. For individual terms, several different methods were tested to evaluate
 188 consistency. These approaches are listed in Table 1, and described in detail in the
 189 respective sections and the Supplemental Information. Method A in Table 1 is the
 190 preferred methodology.

$$(3) \quad \frac{\partial DIC}{\partial t} \Big|_{NCP} = \frac{\left(\frac{\partial TA}{\partial t} \Big|_{Bio} - 2 \times \frac{\partial DIC}{\partial t} \Big|_{Bio} \right)}{\left(-2 + \frac{-17}{117} \right)}$$

$$(4) \quad \left. \frac{\partial \text{DIC}}{\partial t} \right|_{\text{NCC}} = \frac{\left. \frac{\partial \text{TA}}{\partial t} \right|_{\text{Bio}} - \left(\frac{-17}{117} \right) \times \left. \frac{\partial \text{DIC}}{\partial t} \right|_{\text{NCP}}}{2}$$

$$(5) \quad \left. \frac{\partial \text{TA}}{\partial t} \right|_{\text{NCC}} = 2 \times \left. \frac{\partial \text{DIC}}{\partial t} \right|_{\text{NCC}}$$

$$(6) \quad \left. \frac{\partial \text{TA}}{\partial t} \right|_{\text{NCP}} = \left(\frac{-17}{117} \right) \times \left. \frac{\partial \text{DIC}}{\partial t} \right|_{\text{NCP}}$$

Term	Method A	Alternative approaches/Sensitivity tests	
Physical Transport: Lateral advection	Average current, seasonal gradient fit + lateral eddy flux	WHOTS current climatology, gradient climatology + no eddy flux	Average current, gradient climatology + lateral eddy flux
Physical Transport: Eddy Diffusivity	Density gradient	Heat budget	
Evaporation–Precipitation	Salinity budget	Meteorological sensors	Salinity normalization
Mixed Layer Depth	T offset (−0.5°C)	Density offsets (+0.03 kg m ³ , +0.125 kg m ³)	T offset (−1°C)

191 *Table 1. Summary of preferred methodology used for the carbon budget (Method A) and*
 192 *alternative approaches for sensitivity tests of individual terms.*

193 2.2 Total alkalinity and dissolved inorganic carbon

194 The high temporal resolution time-series from the WHOTS mooring sensors between 2004-
 195 2019 is of two carbonate system parameters, seawater pCO₂ (pCO₂sw) and pH. However,
 196 because the seawater pH record has significant data gaps and pH is not an ideal parameter to
 197 pair with pCO₂sw to calculate DIC and TA, we use an alternative approach (McLaughlin et
 198 al., 2015; Sutton et al., 2016). To approximate DIC and TA concentrations at the same
 199 temporal resolution, two steps are necessary. First, a regression of salinity and alkalinity from
 200 HOT cruise surface data, collected at near-monthly frequency, yields a linear regional
 201 salinity-alkalinity relationship. This relationship is then applied to the WHOTS mooring
 202 surface salinity time series, which results in a high-resolution alkalinity time-series. From
 203 measured pCO₂sw and calculated alkalinity, all CO₂ carbonate system parameters, including
 204 DIC, are calculated with the CO2SYS Python package “PyCO2SYS”, an adaptation from the

205 MATLAB version (pyco2sys.readthedocs.io; Humphreys et al., 2022a, b). Constants used are
 206 Sulpis et al. (2020) for carbonic acid and bicarbonate dissociation constants (K_1 and K_2), and
 207 Dickson (1990) for K_{SO_4} . All other values used are the default terms in the PyCO2SYS
 208 package (i.e., default 0 for nutrient concentrations, K_{HF} from Dickson & Riley (1979), and
 209 the boron-chlorinity ratio from Uppström (1974)).

210 2.3 Mixed layer depth

211 Mixed layer depth (MLD) is calculated using a criterion based on a -0.5 °C change in
 212 temperature relative to the temperature at a 10-m reference depth (Sprintall & Tomczak,
 213 1992). This criterion is one of many that is commonly used at Station ALOHA (e.g., Brix et
 214 al., 2004; Keeling et al., 2004). MLD is calculated from the daily average of temperature
 215 profiles measured by WHOTS mooring CTD sensors (sampling every minute at 5-10 m
 216 spacing), interpolated to a one-meter grid. To match the temporal resolution of the budget
 217 calculation, the monthly mean of the daily values is used. Visual inspection of all HOT TA
 218 and DIC profiles used for the analysis indicated that the -0.5 °C temperature threshold most
 219 appropriately captures *in situ* carbon system dynamics compared to other commonly used
 220 criteria (see Figure S1, Movies S1-2 for profiles and MLD). To test for sensitivity of the
 221 analysis to MLD definition, a comparison was made to three other MLD definitions: a -1 °C
 222 temperature threshold (Hastenrath & Merle, 1987), as well as $+0.03$ kg m⁻³ and $+0.125$ kg m⁻³
 223 density thresholds (De Boyer Montégut et al., 2004; Levitus, 1982), all relative to a 10-m
 224 reference depth.

225 2.4 Gas exchange

226 The contribution of gas exchange to monthly DIC change is calculated using wind speed,
 227 SST, salinity, pCO_{2air} and salinity-normalized pCO_{2sw} data all from WHOTS mooring
 228 sensors (Wind speed: <http://uop.whoi.edu/currentprojects/WHOTS/whotsarchive.html>, CTD:
 229 <ftp://mananui.soest.hawaii.edu/pub/hot/whots/>, pCO_2 : Sabine et al., 2012; Sutton et al.,
 230 2012), as well as empirical relationships:

$$(7) \quad \left. \frac{\partial DIC}{\partial t} \right|_{GasExchange} = k \times K_H \times \Delta pCO_2$$

231 Where k is the piston velocity based on wind speeds at 10m above the surface (Liu et al.,
 232 1979), Schmidt number (Wanninkhof, 1992), and a second-order gas transfer
 233 parameterization (Ho et al., 2006), and K_H is the CO₂ solubility constant (Weiss, 1974).
 234 Details on this calculation are listed in the Supplemental Information. All measurements are
 235 averaged hourly, except for the pCO₂sw and pCO₂air data, which is interpolated linearly to
 236 hourly data from measurements taken every three hours. Gas exchange is evaluated hourly
 237 and then averaged monthly.

238 2.5 Physical transport

239 The physical transport term described for DIC in Equation 8, and exactly the same for TA,
 240 comprises horizontal transport, vertical entrainment and diffusion (adapted from Fassbender
 241 et al., 2016, 2017). Individual terms and their units are listed below and in Table 2.

$$(8) \quad \left. \frac{\partial DIC}{\partial t} \right|_{phys} = \left. \frac{\partial DIC}{\partial t} \right|_{Lateral\ transport} + \left. \frac{\partial DIC}{\partial t} \right|_{Entrainment} + \left. \frac{\partial DIC}{\partial t} \right|_{Diffusion}$$

Symbol	Quantity	Calculation/Source	Units
u_{ML}	Average mixed layer current speed	WHOTS mooring sensors. Mean value from monthly averages over the complete WHOTS time-series.	m/s
K_{HOR}	Lateral eddy diffusivity	Zhurbas & Oh (2004).	m ² /s
∇DIC	Horizontal DIC/TA gradient climatologies	Neural networks from World Ocean Atlas climatologies. Broullón et al. (2019), Broullón et al. (2020)	μmol/kg/m
w_{-h}	Vertical velocity at the ML base	Ekman pumping velocity from ASCAT wind stress curl	m/s
K_z	Eddy diffusivity	Climatology based on density gradients at the base of the mixed layer. Keeling et al. (2004)	m ² /s

242 *Table 2. Terms and their units for the physical transport component of the carbon budget.*

243 2.5.1 Lateral transport

244 The complete lateral transport term is calculated as the sum of horizontal background
 245 advection, and lateral eddy transport: $\mathbf{u}_{ML} \cdot \nabla DIC + \kappa_{HOR} \nabla^2 DIC$. For background
 246 advection, current speeds (\mathbf{u}_{ML}) and horizontal gradients in DIC and TA (∇DIC) are
 247 required, while the lateral eddy transport is quantified as a lateral eddy diffusivity (κ_{HOR})
 248 times the Laplacian of DIC and TA fields ($\nabla^2 DIC$).

249 Horizontal fields of TA and DIC have been quantified elsewhere using multiple linear
 250 regression (e.g., Fassbender et al., 2016, 2017) or neural network analysis (e.g., Bittig et
 251 al., 2018; Carter et al., 2018). Climatologies around Station ALOHA from a neural
 252 network are available for both DIC (Broullón et al., 2020) and TA fields (Broullón et al.,
 253 2019). These networks, trained on the GLODAPv2 dataset and then applied to
 254 World Ocean Atlas (WOA) 2013 climatological data, were tested with Station ALOHA
 255 data and proved reliable for predicting TA and DIC in this region. They are used here to
 256 calculate horizontal gradients and the Laplacian of TA and DIC fields.

257 Advection was calculated using the overall mean WHOTS velocity in the mixed layer,
 258 and the mean plus the annual harmonic fit to the DIC and TA gradients from the Broullón
 259 et al. (2019, 2020) climatologies. In situ (WHOTS mooring) current speed measurements
 260 are available at high temporal resolution, but horizontal current speeds at this location are
 261 dominated by mesoscale eddies (Moreno et al., 2022, Figure 3a), which are not resolved
 262 by the large-scale ($1^\circ \times 1^\circ$) and long-term seasonal mean TA and DIC fields. An
 263 investigation into current speed variability revealed that there is no clear annual cycle
 264 (see Figure S3.2). Therefore, the overall mean current speeds with gradient climatologies
 265 best represent the advective component of this budget. The mean zonal component of the
 266 current is westward (-0.04 m s^{-1}), and the average meridional current is northward, but
 267 barely indistinguishable from zero at 0.008 m s^{-1} . This is consistent with well-established
 268 knowledge of large-scale circulation patterns at this location.

269 In order not to neglect the important contribution of mesoscale eddies (see e.g., Barone et
 270 al., 2019), a lateral eddy transport term is added to quantify the influence of the advective
 271 component of mesoscale eddies on the tracer budget. An average lateral eddy diffusivity
 272 from Zhurbas & Oh, (2004) of 8×10^3 is multiplied by the average divergence of the
 273 horizontal gradient field from Broullón et al. (2019, 2020), interpolated to a 2° latitude x
 274 15° longitude grid to reduce noise. For the eddy contribution, a single average value is
 275 used throughout the whole year, while the advective term is at a climatological monthly
 276 resolution based on overall (non-varying) average current speed and an annual harmonic
 277 fit of monthly gradient values. An error of 100% is assigned to the lateral eddy transport.

278 2.5.2 Entrainment and diffusion

279 The entrainment term is the flux through the base of the mixed layer, primarily during
 280 times of local mixed-layer deepening. The relevant upward vertical velocity component is
 281 estimated as monthly mean Ekman pumping from Advanced Scatterometer (ASCAT)

282 daily wind stress curl data (from APDRC: <http://www.apdrc.soest.hawaii.edu/>)_plus
283 changes in mixed layer depth over time (neglecting horizontal advection of the mixed
284 layer gradient). This term is only evaluated for periods of net entrainment; during
285 detrainment, the properties of the water remaining in the mixed layer are not affected by
286 the properties immediately below. Using the sum of these two terms (upward velocity
287 and change over time in MLD), entrainment is then calculated from consecutive HOT
288 cruise profiles in subsequent months and scaled to a monthly value, assuming that the
289 increment of water below the first MLD is mixed into the ML by the time of the
290 following profile. A total of 4 HOT cruise profiles (2%) were excluded due to a mismatch
291 between MLD values and water column DIC/TA data.

292 As for vertical diffusive transport, vertical gradients ($\partial\text{DIC}/\partial z$) are calculated
293 from HOT cruise profiles (again, at near-monthly resolution). The diffusion coefficient or
294 eddy diffusivity (K_z), which governs turbulent diffusion across the bottom of the mixed
295 layer, is not very well constrained due to considerable temporal and spatial variability,
296 and lack of well resolved measurements (Cronin et al., 2015). It is established that
297 turbulent diffusion is orders of magnitude higher in the surface mixed layer than in the
298 thermocline below (e.g., Fernández-Castro et al., 2014). Previous budget or mass-balance
299 based studies of carbon export at this location often used non-varying, representative K_z
300 values (Table S1). However, diffusivity has been shown to vary substantially between
301 seasons (e.g. Cronin et al., 2015). Here, we use a climatology from Keeling et al. (2004)
302 that was calculated from measurements of the vertical density gradient just below the
303 mixed layer.

304 The entrainment term is a composite of true monthly averages and near-monthly profiles,
305 while the diffusive term and the lateral eddy transport term are based on climatological
306 values, and hence do not resolve interannual variability. Physical transport contributions
307 can therefore only be evaluated seasonally.

308 Methods for the sensitivity analysis using alternative approaches (Table 1) for the
309 physical transport term are detailed in the Supplemental Information and include using
310 time-varying current speed climatologies from *in situ* sensors for lateral advection, as
311 well as a heat budget calculation adapted from Cronin et al. (2015) for diffusive transport.

312 2.6 Evaporation – precipitation

313 Adapted from Fassbender et al. (2016, 2017), E–P is determined as the residual of a mixed
314 layer salinity budget (as in equation 8), and then scaled to units of $\mu\text{mol kg}^{-1}$ according to
315 equations 9-10. Additionally, evaporation (E) and precipitation (P) are calculated using two
316 other approaches, to evaluate their consistency and sensitivities: A direct E-P calculation
317 from meteorological sensors, and salinity normalization are described in the Supplemental
318 Information.

$$(9) \quad \left. \frac{\partial Sal}{\partial t} \right|_{E-P} = \frac{\partial Sal}{\partial t} - \left. \frac{\partial Sal}{\partial t} \right|_{Phys}$$

$$(10) \quad \left. \frac{\partial DIC}{\partial t} \right|_{E-P} = \left. \frac{\partial Sal}{\partial t} \right|_{E-P} \times \left. \frac{DIC}{Sal} \right|_{t=0}$$

319 2.7 Error analysis

320 The error of the linear alkalinity-salinity fit is estimated as the standard error of the estimate
 321 (equation 11). The uncertainty of high-resolution DIC is evaluated using the error
 322 propagation tool of CO2SYS (Orr et al., 2018). Assigned uncertainties – the SE of calculated
 323 TA, as well as measurement errors for remaining parameters – are reported in Table 3.

$$(11) \quad SE = \sqrt{\frac{\sum(TA_{meas} + TA_{calc})^2}{N - 2}}$$

Quantity	Error	Source
Total Alkalinity	4.95 μmol kg ⁻¹	Standard Error
DIC	7.7 μmol kg ⁻¹	CO2SYS error propagation (Orr et al., 2018)
Temperature	0.002 °C	Reported by manufacturer (Sea-Bird Scientific)
Salinity	0.012	Mandujano et al. (2016)
pCO _{2sw}	2 μatm	Sutton et al. (2014)
pCO _{2air}	1 μatm	Sutton et al. (2014)
MLD (h)	2.4 m	¼ of vertical separation of sensors (Fassbender et al., 2016)
Piston velocity (k)	30%	Nightingale et al. (2000), Fassbender et al. (2016)
Wind speed	0.1 m/s	https://journals.ametsoc.org/view/journals/atot/37/4/jtech-d-19-0132.1.xml
Carbon quotient in Redfield ratio	14	Anderson & Sarmiento (1994)
Turbulent eddy Diffusivity (Kz)	2.2 x 10 ⁻⁵	Standard deviation of climatological means
Lateral eddy transport	100%	Assigned since there are no uncertainties reported for K _{LAT}

Mean mixed layer current speeds (u_{ML})	0.008 m s ⁻¹	SEM (from autocorrelation analysis)
--	-------------------------	-------------------------------------

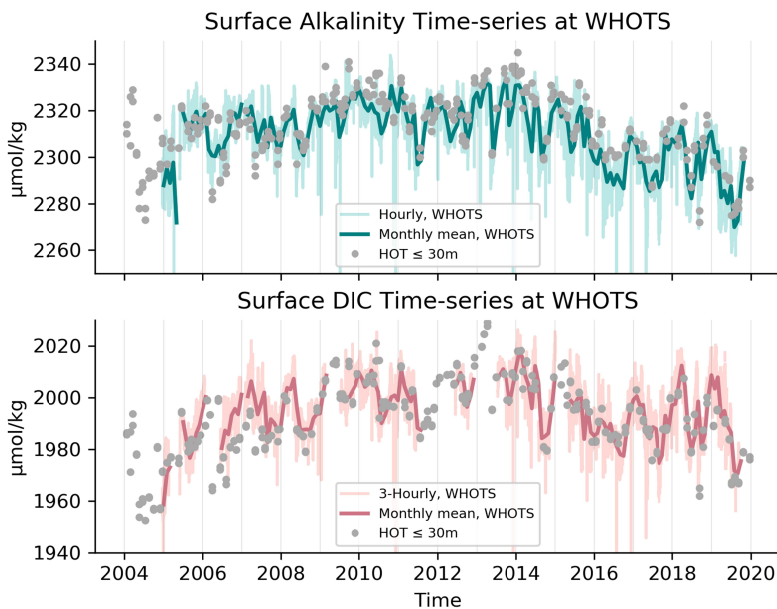
324 *Table 3. Error estimates for Monte Carlo analysis and their sources.*

325 **3 Results**

326 3.1 Surface DIC and TA time-series

327 A regression of total alkalinity and salinity in the top 30m provided a well-constrained
 328 relationship between the two parameters ($R^2 = 0.89$, $n = 630$), and a standard error of the
 329 estimate of $4.95 \mu\text{mol kg}^{-1}$, (Equation 12). The propagated error (standard error propagation
 330 in CO2SYS) in DIC, calculated from this estimated TA and measured $p\text{CO}_{2sw}$ is $7.7 \mu\text{mol}$
 331 kg^{-1} . There is good agreement between HOT discrete observations of both TA and DIC with
 332 the calculated time-series of these parameters, with mean residuals of $4.0 \mu\text{mol kg}^{-1}$ for TA
 333 (discrete > calculated) and $-1.7 \mu\text{mol kg}^{-1}$ for DIC (discrete < calculated), which fall within
 334 the uncertainty estimates (see Figure 2).

$$(12) \quad TA = 66.68 * S - 29.73$$



335

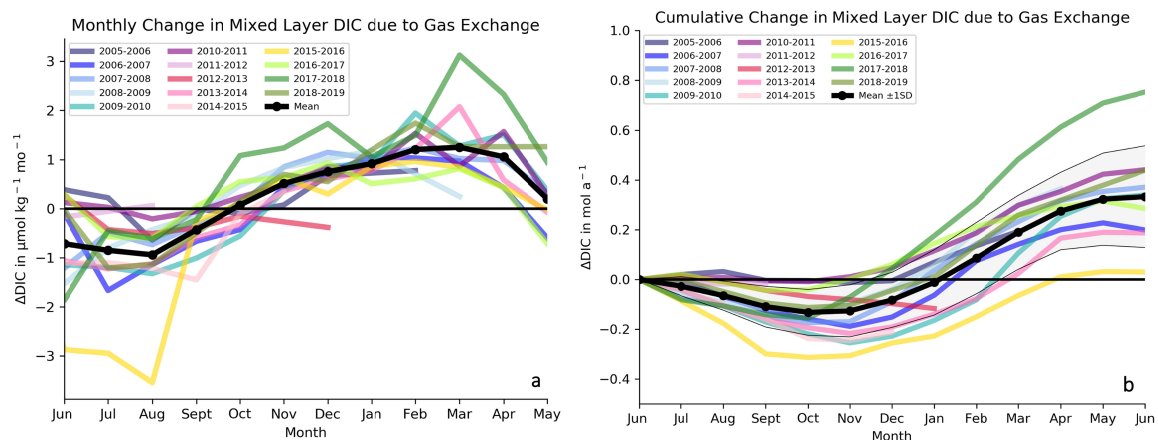
336 *Figure 2. Surface alkalinity and DIC time-series at the WHOTS mooring, comparing upper*
 337 *30m discrete HOT samples with monthly means from calculated high-resolution (3-hourly)*
 338 *mooring-based data.*

339 3.2 Gas exchange

340 Since the whole gas exchange term is resolved at hourly frequency, we can calculate true
 341 monthly averages of this term, enabling evaluation not just of a seasonal climatology, but of
 342 changes from monthly to interannual time scales. High confidence in the monthly mean

343 values is confirmed by the small variance between Monte Carlo runs (see uncertainty in
344 Table 3).

345 Gas exchange contributes relatively little to mixed layer DIC variability, with maxima for
346 individual months of +3 and -4 $\mu\text{mol kg}^{-1} \text{mo}^{-1}$ (corresponding to a climatological maximum
347 CO_2 flux of +3.7 $\text{mmol m}^{-2} \text{d}^{-1}$ for March, and a minimum of -1.8 $\text{mmol m}^{-2} \text{d}^{-1}$ in
348 September) (Figure 3a). The seasonal cycle is distinctive, with increasing DIC through Dec-
349 May (uptake) and decreasing DIC in Jul-Oct (outgassing) (Figure 3a), confirming previous
350 studies on time periods of source and sink behavior over the year (e.g., Sutton et al., 2017).
351 Cumulative DIC change due to gas exchange is positive for each complete deployment year
352 (June to June). An exception is the strong El Niño year 2015-2016, where an intense
353 outgassing period in August and September 2015 yields a 2015-2016 DIC change from gas
354 exchange that is virtually indistinguishable from zero. The average net annual uptake is 0.37
355 mol C m^{-2} from gas exchange at this location (Figure 3b).



356
357 *Figure 3. Change in mixed layer DIC due to gas exchange, both monthly averages in*
358 *concentration change (3a), and total cumulative inputs over a year in mol C (3b).*

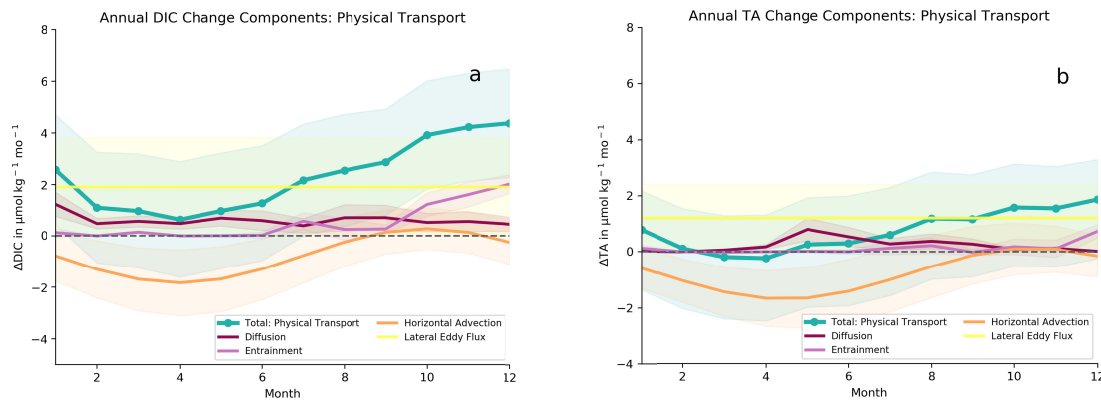
359 3.3 Evaporation – precipitation

360 The average E-P is close to zero over a year for both DIC and TA, with net evaporation
361 between June-October (except for August) and oscillating positive and negative values for
362 the rest of the year (see Figure S4).

363 3.4 Physical transport

364 The physical transport term cannot be evaluated for interannual variability, as the lateral eddy
365 flux divergence is approximated as a constant and the diffusive flux is based on a vertical
366 eddy diffusivity (K_z) seasonal climatology. DIC changes from physical transport are
367 positive, averaging about 2.5 $\mu\text{mol kg}^{-1}$ per month with a maximum of just under 5 $\mu\text{mol kg}^{-1}$
368 in December, and a minimum of $\sim 1 \mu\text{mol kg}^{-1}$ in March (Figure 4a). Vertical diffusion
369 supplies small positive inputs throughout the year, and there is a distinctive $\sim 2 \mu\text{mol kg}^{-1}$
370 entrainment signal between October-December. There is a seasonal pattern in non-eddy
371 horizontal transport, with removal of DIC throughout most of the year, as low-DIC waters
372 are advected from the East (and, to a much smaller extent, from the South), except from

373 September-December where fluxes are slightly positive with high-DIC waters advected from
 374 the East. The largest contribution in addition to the entrainment signal is the yearly average
 375 lateral DIC flux divergence from mesoscale eddies, which is about $2 \mu\text{mol kg}^{-1} \text{mo}^{-1}$, mainly
 376 due to the meridional component of flux divergence. The physical transport term for TA is
 377 similar to that of DIC, but smaller (mean: $<1 \mu\text{mol kg}^{-1} \text{mo}^{-1}$, maximum: $2 \mu\text{mol kg}^{-1} \text{mo}^{-1}$ in
 378 December), due to both a smaller entrainment peak and a smaller lateral eddy transport term
 379 ($\sim 1 \mu\text{mol kg}^{-1} \text{mo}^{-1}$). Throughout the first half of the year, stronger TA losses from the non-
 380 eddy horizontal transport term in conjunction with smaller positive fluxes from the other
 381 terms yield overall (small) negative or near-zero values (Figure 4b).

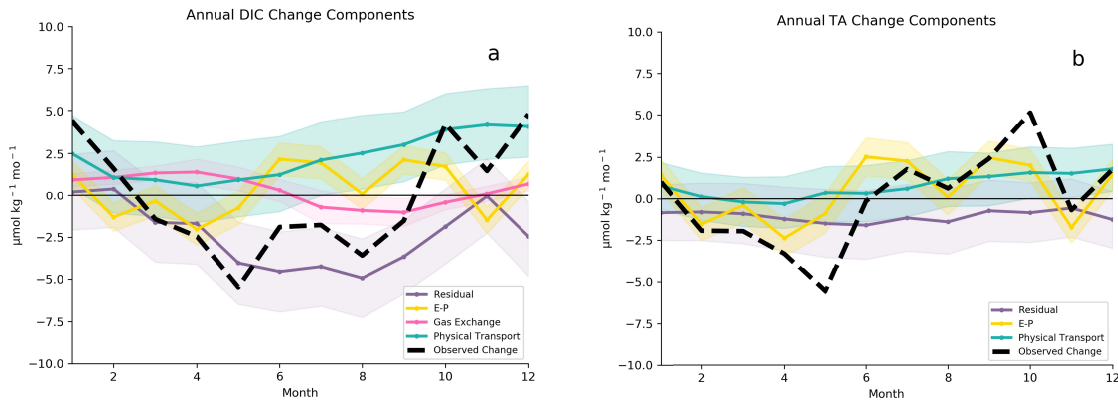


382

383 *Figure 4. Yearly climatology of the physical transport term and its components for DIC (4a)*
 384 *and TA (4b). Shaded areas correspond to ± 1 standard deviation of Monte Carlo runs.*

385 3.5 Biological term

386 The seasonal cycle of all budget terms and the observed change are shown in Figure 5. The
 387 residual contains all biological processes, as well as the errors of all other terms and any
 388 processes that are unaccounted for. The residual term for Method A closely matches the
 389 observed seasonal DIC cycle (Figure 5a), while the observed TA largely tracks the E–P term
 390 (Figure 5b), stressing the importance of concentration/dilution for TA and of biological
 391 processes for DIC over an annual cycle. The strong DIC drawdown from biological
 392 productivity and excess precipitation in the spring is balanced by DIC supply from physical
 393 transport and ingassing. A secondary peak in drawdown in the later summer is also opposed
 394 by a larger positive physical transport input, as well as additional excess evaporation, but
 395 accentuated by outgassing during the same period. Most of the observed TA seasonal cycle is
 396 explained by the E–P term, leaving a biological TA drawdown to compensate for the largely
 397 positive inputs from physical transport over a year.



398

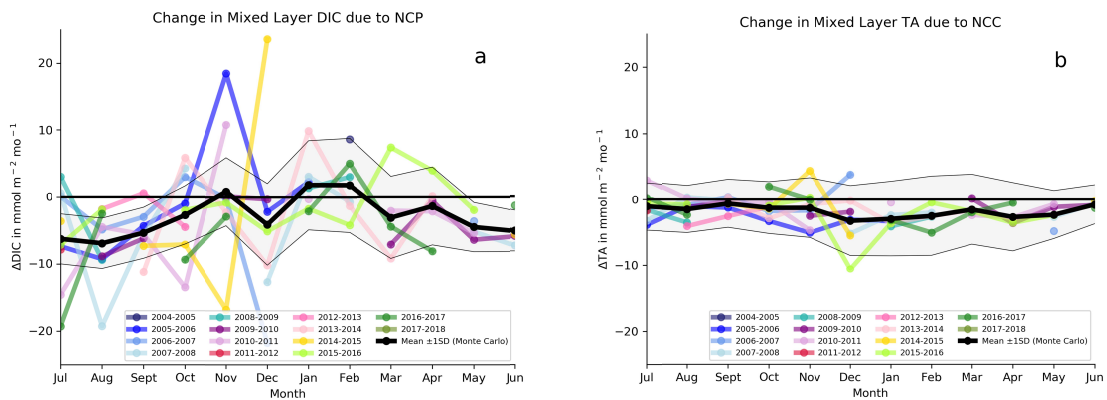
399 *Figure 5. Yearly climatology of the biological term (residual of the budget) and model input*
 400 *terms for DIC (5a) and TA (5b). Shaded areas correspond to ± 1 standard deviation of*
 401 *Monte Carlo runs.*

402 3.6 NCP and NCC

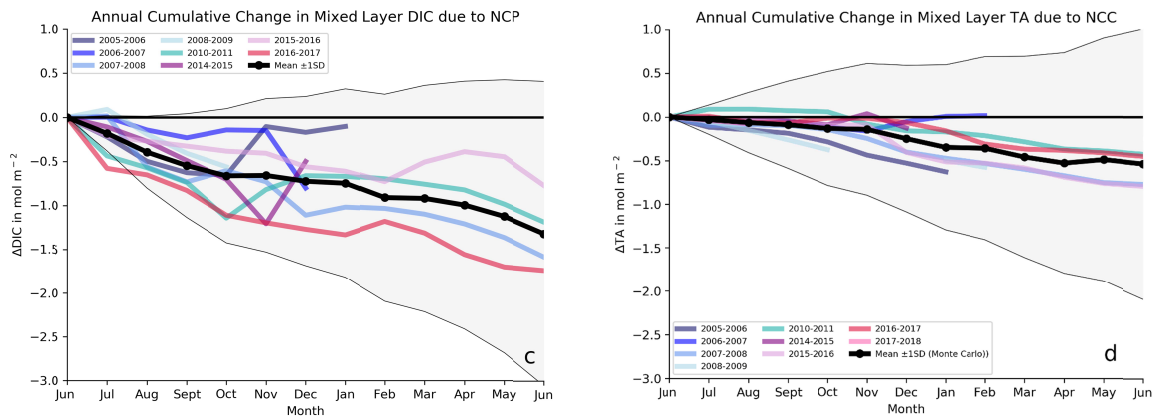
403 Figure 6 displays the seasonal cycle in NCP and NCC contributions to DIC and TA change,
 404 the two processes that compose the biological term.

405 The ocean at Station ALOHA is net autotrophic over the annual mean, with NCP close to
 406 zero between October and February, and relatively consistent net autotrophy (DIC loss) of
 407 about 7 mmol mo^{-1} between March and September, as well as in January (Figure 6a). The
 408 cumulative average DIC (aNCP) loss from NCP is 1.5 mol m^{-2} (Figure 6c).

409 TA drawdown from net calcification largely occurs in the winter and spring, between
 410 December and April, with values close to zero in the remaining months yielding net
 411 calcification (TA loss) over a year (Figure 6b). Cumulative NCC (aNCC) was 0.6 mol m^{-2} of
 412 TA drawdown (Figure 6d).



413



414

415 *Figure 6. Yearly climatology of mixed layer NCP and NCC rates (6a,b), and (cumulative)*
 416 *aNCP and aNCC (6c, d), as well as averages for each year. Shaded area represents ± 1*
 417 *standard deviation of Monte Carlo runs. Only complete years shown for 6c, d.*

418 **4 Discussion**

419 **4.1 Discrepancies and sensitivity tests**

420

Study	Method	Time	Depth	aNCP (- mol C m ⁻² yr ⁻¹)	(mean) NCP rate (- mmol C m ⁻² d ⁻¹)
Emerson et al. (2008) ^a	O ₂ /Ar budget	2004 –2005	ML	-4.2 ± 1.9	-11.5 ± 5.2
Keeling et al. (2004)	Diagnostic box model (DIC & δ ¹³ C)	1988 –2002	ML	-2.2 ± 0.8	-6.0 ± 2.2
Lee (2001) ^a	DIC change	Summer 1990	ML	-2.3 ± 0.8	-6.3 ± 2.2
Quay et al. (2009) ^a	Carbon budget (DIC & δ ¹³ C)	2004 –2005	ML	-2.4 ± 1.0	-7.85 ± 2.19
Quay et al. (2010) ^a	O ₂ /Ar budget	2006 –2007	ML	-3.7 ± 1.0	-10.1 ± 2.7
Quay & Stutsmann (2003)	Carbon budget (DIC & δ ¹³ C)	1994 –1999	ML	-2.3 ± 1.3	-6.3 ± 3.4
Wilson et al. (2015)	Prior O ₂ /Ar-NCP	Jul-12	ML	-	-6.0 ± 3.2
Wilson et al. (2015)	Prior O ₂ /Ar-NCP	Aug-12	ML	-	7.6 ± 4.2
Wilson et al. (2015)	Prior O ₂ /Ar-NCP	Aug – Sep 2012	ML	-	0.5 ± 3.1
Sonnerup et al. (2013) ^a	CFC/SF ₆ model	2008	Winter ML	-2.5 ± 3.0	-6.8 ± 8.2
Yang et al. (2017) ^a	O ₂ budget	2014 –2018	Winter ML	-2.4 ± 0.6	-6.6 ± 1.6
Emerson et al. (1995) ^a	O ₂ /Ar/N ₂ budget	1990	0-100m	-1.0 ± 0.7	-2.7 ± 1.9

Emerson et al. (1997) ^a	O ₂ /Ar/N ₂ budget	Early 1990s	0-100m	-2.7 ± 1.7	-7.4 ± 4.7
Sonnerup et al. (1999) ^a	CFC model	1991	0-100m	-2.2 ± 0.5	-6.0 ± 1.4
Hamme & Emerson (2006) ^a	O ₂ /Ar/N ₂ budget	2000 – 2001	0-115m	-1.1 ± 0.5	-3.0 ± 1.4
Benitez-Nelson et al. (2001)	²³⁴ Th / ²³⁸ U disequilibrium	1999 – 2000	0-150m	-1.5 ± 0.8	-4.0 ± 2.3 (PC flux)
Brix et al. (2006)	Diagnostic box model (DIC & δ ¹³ C)	1989 – 2000	0-150m	-3.1 ± 0.3	-8.5 ± 0.8
Ferrón et al. (2021)	O ₂ /Ar	2014 – 2018	0-150m	-1.5 ± 0.4	-4.1 ± 1.1
Riser & Johnson (2008) ^a	O ₂ budget	2002 – 2005	0-150m	-1.6 ± 0.2	-4.4 ± 0.5
Emerson (2014)	Average of literature values	-	-	-2.5 ± 0.7	-6.8 ± 1.9
<i>This study</i>	<i>Carbon budget (DIC & TA), Method A</i>	<i>2005 - 2019</i>	<i>ML</i>	<i>-1.5 ± 1.7</i>	<i>-3.4 ± 2.8</i>

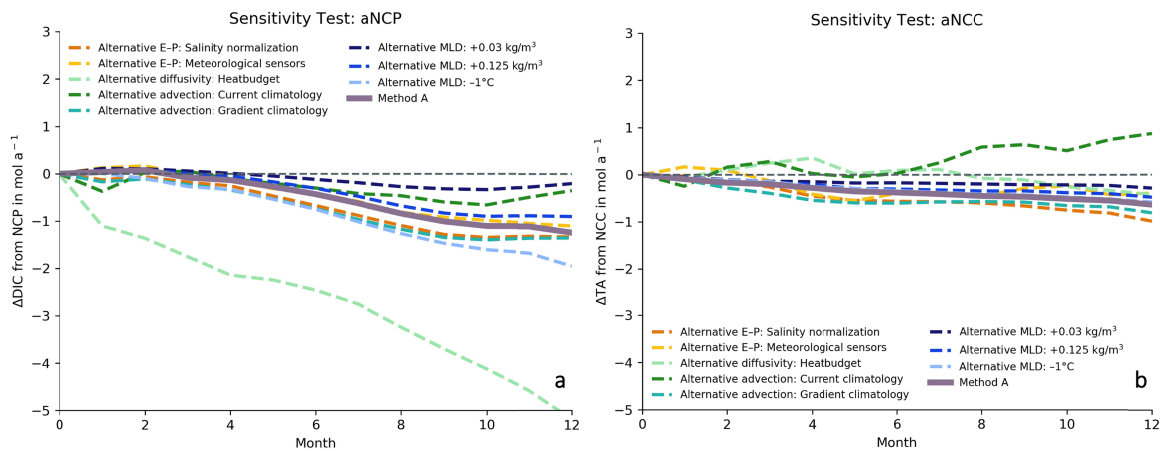
421 *Table 4. Literature comparison of average NCP rates and aNCP values at Station ALOHA.*
 422 ^a – adapted from Ferrón et al., (2021).

423

Study	Term	Value	Units
Karl et al. 2021	Average HOT PIC flux 2001-2019	24.2	mg CaCO ₃ m ⁻² d ⁻¹
		2.9	mg C m ⁻² d ⁻¹
Dong et al. 2019	CaCO ₃ flux near ALOHA @100m depth	71.1	mg CaCO ₃ m ⁻² d ⁻¹
		8.5	mg C m ⁻² d ⁻¹
Betser et al. 1985	Pteropod (aragonite) fluxes at 100m. 21°N, Western North Pacific	32.6	mg CaCO ₃ m ⁻² d ⁻¹
		3.9	mg C m ⁻² d ⁻¹
Sabine 1995a	Carbonate flux from dissolution	40	mg CaCO ₃ m ⁻² d ⁻¹
		4.8	mg C m ⁻² d ⁻¹
Sabine & Mackenzie 1995	Sediment trap CaCO ₃ flux - HOT-7 200m	40.3	mg CaCO ₃ m ⁻² d ⁻¹
		4.8	mg C m ⁻² d ⁻¹
Sabine & Mackenzie 1995	Sediment trap CaCO ₃ flux - HOT-9 200m	40.7	mg CaCO ₃ m ⁻² d ⁻¹
		4.8	mg C m ⁻² d ⁻¹
Sabine & Mackenzie 1995	Sediment trap CaCO ₃ flux - HOT-11 200m	39.4	mg CaCO ₃ m ⁻² d ⁻¹
		4.7	mg C m ⁻² d ⁻¹
Sabine & Mackenzie 1995	Sediment trap CaCO ₃ flux - HOT-15 200m	40.8	mg CaCO ₃ m ⁻² d ⁻¹
		4.9	mg C m ⁻² d ⁻¹
<i>This study</i>	<i>Mean mixed layer TA change from NCC</i>	<i>170</i>	<i>mg CaCO₃ m⁻² d⁻¹</i>
		<i>20.4</i>	<i>mg C m⁻² d⁻¹</i>

424 *Table 5. Literature comparison of average carbonate fluxes at Station ALOHA in different*
 425 *units.*

426 Results of this study are on the lower end of the reported range for aNCP at this location (1.5
 427 vs mean 2.0 mol m⁻², see Table 4.1). However, given error estimates here and in previous
 428 studies, none of the aNCP estimates are significantly different from the results presented here
 429 (see Table 4). By contrast, average aNCC is four to seven times larger than HOT sediment
 430 trap results, which constitute the only available dataset with which to compare (Table 5).
 431 Sediment traps are known to provide a lower-end estimate for PIC and PC export fluxes, but
 432 an inorganic carbon flux making up 30% of total carbon export is likely to be an
 433 overestimation at this site. A sensitivity analysis investigating different methodologies to
 434 quantify most of the terms of this carbon budget can shine a light on the origins of and
 435 insights from the divergence we see in average aNCP, and especially aNCC values compared
 436 to previous reports. The alternative methods used for E–P, horizontal transport, and diffusion
 437 terms are listed in Table 1 and expanded upon in the Supplemental Information. Figure 7
 438 shows NCP and NCC calculated using these methods.



439
 440 *Figure 7. Sensitivity test for all different methodologies showing resulting Monte Carlo*
 441 *average aNCP (7a) and aNCC (7b).*

442 4.1.1 Gas exchange

443 Annual CO₂ invasion here is 0.37 mol m². This estimate is much lower than previous
 444 estimates based on pCO₂ calculated from discrete TA and DIC measurements (e.g. Quay
 445 & Stutsman (2003): 0.6 ± 0.4 mol C m⁻², Dore et al. (2009): ~0.5 mol C m⁻²), and
 446 underway pCO₂ data (Takahashi et al., 2009) but equivalent to earlier estimates from the
 447 WHOTS mooring (Sutton et al., 2017). A discrepancy between WHOTS flux estimates
 448 and underway pCO₂ systems was previously reported as 60%, and explained partly by
 449 differences in wind speed parameterization (Sutton et al. (2017)). Additionally, there is
 450 an average offset of about 8 μatm in measured pCO₂ at the WHOTS mooring compared
 451 to calculated pCO₂ from HOT measurements, which is small (2% of the mean) but grows
 452 considerably when integrated over time such as in integrated annual flux calculations.
 453 Possible contributors to this offset include differences in temperature (and therefore
 454 pCO₂) due to measuring depth (<1m for WHOTS, 5-30m for discrete data), conditions

455 within the mooring measurement apparatus (equilibrator) not representing mean mixed
456 layer pCO₂, or a systematic underestimation of pCO₂ calculated from TA & DIC. For this
457 budget, both underestimated ingassing in the spring/summer and overestimated
458 outgassing in the fall would entail underestimated NCP rates for these same months, and
459 could partly be responsible for the relatively low aNCP reported here. Additionally, since
460 for this budget CO₂ invasion is converted to a concentration change and then integrated
461 over the mixed layer, the choice in mixed layer depth definition also impacts the gas
462 exchange term, with a shallower mixed layer accentuating both outgassing and ingassing
463 signals (see Figure S4b).

464 4.1.2 Horizontal transport

465 The contribution of advection and diffusion to the DIC budget has been unclear in both
466 magnitude and seasonality in previous studies (Dore et al., 2014, 2009; Keeling et al.,
467 2004). Despite the extraordinarily abundant data from the long-standing Hawaii Ocean
468 Time-series project, the high-resolution data needed in both time and space to accurately
469 quantify physical transport fluxes of carbon species has not been available. Nonetheless,
470 progress in quantifying both horizontal and vertical inputs of DIC and TA may be
471 possible by using newer data products including the high temporal resolution WHOTS
472 mooring current speeds and horizontal gradient climatologies from neural networks
473 (Broullón et al., 2019, 2020).

474 Unfortunately, data availability for horizontal gradients and eddy diffusivity still restricts
475 us to a *seasonal* budget. The effect of using a time-varying current speed climatology
476 instead of average current speeds to constrain horizontal transport illustrates a basic
477 problem with using a seasonal budget approach at this location, where seasonality
478 explains only a small fraction of the variability. For both DIC and TA, interannual
479 variability is much larger than the amplitude of a seasonal cycle, with a variance in
480 monthly averages of about 30-50 $\mu\text{mol kg}^{-1}$ between years, but an average seasonal cycle
481 of only about 15 $\mu\text{mol kg}^{-1}$. As discussed in the methods section, current speeds at this
482 location are dominated by mesoscale eddies, and also do not vary strongly with season at
483 Station ALOHA (see Figure S3.2).

484 For a sensitivity check, using a current speed climatology from WHOTS ADCPs, instead
485 of the average current speed used in Method A, drastically changes the horizontal
486 transport term for TA and DIC (Figure S4), and consequently also NCC and NCP (Figure
487 7b). This is mainly based on the average direction of transport for individual months of
488 the current climatology (Figure S2). However, this average direction does not represent
489 any “real” seasonality in current speed and direction, as the currents have been shown to
490 have no significant seasonality (Figure S3) – so the seasonality of the modified advective
491 term is questionable. At locations of previous studies using this approach (Fassbender et
492 al., 2016, 2017), horizontal contributions to the overall carbon budget were negligible or
493 small compared to other budget components. Due to a much smaller contribution of
494 vertical mixing and entrainment, at this location the advective term becomes the most
495 important physical transport process (Figure 4). It is therefore likely that the discrepancy
496 between NCP & NCC calculated here and literature values can partly be explained by the
497 inability to meaningfully evaluate this important term on a seasonal time-scale.

498 This illustrates the need for data on horizontal gradients of surface carbonate chemistry
499 parameters at higher spatiotemporal resolution, as will hopefully be achieved by
500 promising current and future endeavors using floats, autonomous vehicles, and satellites
501 (e.g., Nicholson et al., 2022; Nickford et al., 2022). With data on variability in TA/DIC
502 gradients at the spatiotemporal scale of mesoscale eddies, the construction of a carbon
503 budget at the appropriate time scale(s) would be possible, and the importance of
504 horizontal transport for carbon cycling at this location could be investigated.

505 The annual cycle calculated here using Method A shows advective DIC and TA loss
506 especially in the early spring (DIC) and summer (TA), driven by a small zonal
507 component of the gradient, both parameters increasing to the west. Interestingly, previous
508 studies have neglected zonal transport due to the small gradients (e.g., Dore et al., 2009,
509 Keeling et al., 2004), and indeed meridional gradients in DIC and TA are much steeper
510 throughout the year, with both parameters increasing northward (see Supplemental
511 Information, Figure S3c-d). However, the weak mean meridional flow (average 0.008 m s^{-1})
512 contributes only a small loss, the net advective term is dominated by the stronger
513 mean zonal flow acting on the seasonally varying zonal gradient.

514 4.1.3 Vertical transport

515 For the vertical transport term, a heat budget based on Cronin et al. (2015) was
516 constructed to constrain eddy diffusivity in a different way (see Supplemental
517 Information). Since there are order of magnitude differences in the climatological
518 diffusivity values generated by the Keeling et al. (2004) and the Cronin et al. (2015)
519 approach, a sensitivity analysis to the choice of diffusivity coefficients was performed.
520 Generally, due to increasing DIC with depth (a positive vertical DIC gradient), higher K_z
521 will lead to increased diffusive DIC fluxes into the mixed layer, which, in turn,
522 propagates to a larger biological term and more DIC drawdown from NCP (essentially
523 balancing higher K_z input values). For TA, the relationship is less straightforward due to
524 an alkalinity maximum associated with the North Pacific Tropical Water (NPTW) at
525 Station ALOHA that varies in location relative to the mixed layer (Lukas & Santiago-
526 Mandujano, 2008). Both time-varying K_z estimates show a peak in diffusive transport in
527 the spring, and the shape of the annual cycles is remarkably similar, but they differ by an
528 order of magnitude across their whole range (Figure S5). The Keeling et al. (2004) data is
529 more in line with literature data, and the calculation based on the heat budget yields
530 (unrealistic) negative values indicating up-gradient transport in the fall. As Table S3
531 shows, the choice of K_z values strongly impacts the final NCP and NCC results,
532 especially in the springtime when biological drawdown of DIC is most prevalent.
533 Therefore, more measurements and refined budget calculations using float and mooring
534 data to constrain K_z values at various temporal and spatial scales would be very useful for
535 biogeochemical tracer budgets such as this one.

536 4.1.4 Evaporation – precipitation

537 E–P using a salinity budget (Method A) vs. salinity normalization are very similar, while
538 the calculation based on WHOTS measurements yields much smaller fluxes (Figure S4,
539 S5). They all converge on (maximum) net evaporation during the summer/fall, between

540 June and October. With the direct calculation from mooring sensors, net evaporation
541 persists throughout the year, while the other two approaches largely indicate net
542 precipitation earlier in the year (Feb-May). The large discrepancy between the salinity-
543 based and the directly measured approaches can partly be explained by rainfall
544 measurements. Mooring precipitation sensors do not match satellite, shipboard or model
545 results, largely due to the extreme patchiness of rainfall.

546 However, it is also likely that unresolved advective processes affect the salinity-based
547 calculation, but that those contributions are cancelled out in the final carbon budget. The
548 residual of the salinity budget contains all errors and fluxes that are not accounted for in
549 the physical transport terms. E-P is the residual of the salinity budget, and appears to be
550 driving most of the observed salinity variations; this suggests an underestimation of
551 physical transport terms, as local precipitation and evaporation are not expected to be the
552 main control of sea surface salinity. We assume that any unresolved processes affecting
553 salinity are essentially conservative mixing processes (i.e., they affect TA and DIC
554 proportionally), such as advection of regional gradients in salinity (and TA, DIC) from
555 local precipitation differences that are not captured by $1^{\circ}\times 1^{\circ}$ climatological fields.
556 Consequently, the use of the salinity budget for the E-P term is beneficial for the final
557 carbon mass balance. Since the (scaled) salinity physical transport term is subtracted
558 from the DIC/TA physical transport terms, any biases that they both exhibit should cancel
559 out, similarly as discussed in Fassbender et al. (2016, Equation 10); while this shows
560 again that the physical transport term taken alone is likely not resolving important
561 contributions, this increases the confidence in final NCC and NCP values.

562 4.1.5 Mixed-layer depth

563 Several definitions of mixed layer depth have been used at Station ALOHA, including the
564 density criteria of $+0.03 \text{ kg m}^{-3}$ from De Boyer Montégut et al. (2004) (e.g. Ferrón et al.,
565 2021; Barone et al., 2019; Karl et al., 2021), and 0.125 kg m^{-3} from Levitus (1982) (e.g.,
566 Dore et al., 2003, 2009, 2014; Quay & Stutsman, 2003; Wilson et al., 2015), as well as
567 the temperature criterion of -1°C from Hastenrath & Merle (1982) (e.g. Venrick, 1993;
568 Cortés et al., 2001). All MLD criteria yield very similar NCC estimates. While the
569 general shape of the seasonal DIC changes from NCP is the same for all MLD estimates,
570 the magnitude of these fluxes varies more between different estimates, leading to
571 differences of cumulative aNCP from 0.25 mol m^{-2} using the $+0.03 \text{ kg m}^{-3}$ density
572 criterion (shallower ML definition) to $\sim 2 \text{ mol m}^{-2}$ using a -1°C temperature threshold
573 (deeper ML definition). Although all of these estimates are within the aNCP error, this
574 illustrates the importance of MLD definition for mixed layer carbon budgets.

575 It is worth mentioning that discrepancies between multiple approaches to some of these terms
576 could only be exposed due to the unusual abundance of various complementary and
577 redundant datasets at Station ALOHA, and could have easily gone unnoticed in other
578 locations with less available data. There are issues with constraining seasonal fluxes of
579 several key contributors to the carbon budget at this location compared to other studies, but
580 the challenges adapting this approach are interesting results themselves: At Station ALOHA,
581 where seasonal changes in mixed layer depth and stratification are much smaller than in the
582 temperate ocean, constraints on (horizontal) transport from mesoscale eddies at the

583 appropriate spatial resolution become a crucial ingredient for an accurate mixed layer carbon
584 budget, and depending on MLD definition, NCP can differ by about 100%. Additionally, and
585 nonetheless, valuable insights can be gained from the budget components and final
586 aNCC/aNCP estimates obtained from the most reliable (Method A) combination of
587 methodologies, including a comparison of identified drivers of the seasonal carbon cycle and
588 their relative contributions and timing to previously published studies.

589 4.2 Drivers of the seasonal carbon cycle

590 Previous studies that utilized carbon budget models at Station ALOHA either constrained
591 vertical diffusive fluxes and inferred horizontal transport (Keeling et al., 2004), or vice versa
592 (Quay & Stutsman, 2003), with results varying considerably based on these assumptions.
593 According to Keeling et al. (2004), the main processes behind mixed layer DIC variability
594 are biological productivity, gas exchange and horizontal transport, as well as a period of
595 winter entrainment. There is agreement that the largest signal is a summer drawdown of
596 (salinity normalized) DIC due to biological activity (Quay & Stutsman, 2003; Keeling et al.,
597 2004). The amplitude of this seasonal DIC drawdown is dampened, because gas exchange is
598 strongest around the same time, but acts in opposite direction: The air to sea flux is highest in
599 spring (around April), when NCP strongly decreases mixed-layer DIC (Keeling et al., 2004).
600 These observations are largely confirmed by this study, with a small difference in timing.
601 Maximum ingassing occurs in March-April, and maximum drawdown from NCP in May-
602 Aug (Figure 6a). This is consistent with a peak in primary productivity later in the spring due
603 to increased light and nutrient availability (from deepening PAR attenuation and a shoaling
604 nutricline), and potential contribution from nitrogen-fixing cyanobacteria that are known to
605 bloom with increasing stratification in the late summer (e.g., Karl & Church, 2017). The
606 main processes that dampen the spring DIC drawdown here are physical transport, as well as
607 ingassing of DIC between March-May, both at about $1\text{-}2\ \mu\text{mol kg}^{-1}\ \text{mo}^{-1}$. Later in the
608 summer, the continued biological DIC drawdown from NCP is enhanced by outgassing of
609 DIC, but dampened by excess evaporation and by increased physical transport inputs.

610 In a recent study on net community production at Station ALOHA from oxygen dynamics,
611 Ferrón et al. (2021) reported lower NCP rates between December and February, followed by
612 an increase through June and then mostly high values (i.e., net autotrophy) through
613 November. In this study, the NCP increase starts later, from Apr-Jun, and we observe a shift
614 to near- zero NCP by October. Ferrón et al. (2021) suggest that their NCP_{ML} values in the
615 late fall might be too high and suggest correcting for entrainment diffusive fluxes of oxygen
616 by up to 65-100% for individual months between Sep-Nov, which would lead to a 12%
617 reduction in their aNCP estimate.

618 Studies on calcium carbonate production and dissolution at Station ALOHA and in the NPSG
619 are relatively sparse. Some studies in the 1980s and 1990s (e.g., Betser et al., 1984; Sabine et
620 al., 1995; Sabine & Mackenzie, 1995). Sabine & Mackenzie (1995) reported an export of
621 around $40\text{mg CaCO}_3\ \text{m}^{-2}\ \text{d}^{-1}$, and interestingly first detected the presence of calcium
622 carbonate particles from benthic, more soluble calcifying organisms living on shallow, near-
623 coastal banks in the water column at this location. To our knowledge, so far there have been
624 no attempts to quantify seasonal variability in calcification/dissolution and CaCO_3 export
625 dynamics at Station ALOHA. Cortés et al. (2001) studied the ecology of coccolithophores, an

626 important calcifying phytoplankton, and found extremely low abundances throughout most
627 of the year. Only during March and September/October, a fairly specific range of
628 environmental conditions regarding temperature (20-25°C), salinity (34.9-35.2), nutrients
629 (0.004-0.07 μmol/kg nitrate, <0.025 μmol/kg phosphate), and light availability (2-25 μE m⁻² s⁻¹)
630 appears to enable these higher cell densities (Cortés et al., 2001). Only a very small
631 fraction of zooplankton at Station ALOHA was reported to be made up of shelled pteropods
632 (Steinberg et al., 2008), but they are likely a significant contributor to PIC export due to their
633 large size. Foraminifera, calcifying zooplankton, were examined by Monteagudo (2016)
634 using bottom-moored sediment traps, and found to be more abundant during the summer
635 months. Boeuf et al. (2019) investigated species composition of particles retained in deep sea
636 sediment traps, and found foraminifera to be sporadically present in large concentrations, and
637 pteropods generally abundant in deep sea particles. The sparse information on these three
638 most important groups of calcifying organisms illustrates the highly variable nature of PIC
639 export at Station ALOHA for each of them, highlighting the need for more species-specific
640 studies of these organisms and the drivers of associated export events.

641 **5 Conclusions and outlook**

642 This study is a first attempt to quantify seasonality in calcification/dissolution dynamics at
643 Station ALOHA, and results show annual net calcification of 0.5 mol m⁻². This exceeds all
644 previously reported fluxes from sediment trap data, with maximum export occurring during
645 December-April.

646 The mixed layer ecosystem at Station ALOHA is confirmed to be net autotrophic over a year, at
647 about 1.5 mol C m⁻². Biological drawdown during March-September exceeds the inputs from
648 physical transport processes, which are positive throughout the year with a distinct fall-winter
649 peak. Contributions to DIC changes from evaporation and precipitation and gas exchange show
650 clear opposing seasonal cycles.

651 At Station ALOHA, it would be particularly beneficial to resolve more than the annual cycle of
652 carbon parameters, as variability on other time-scales is large compared to seasonal variations.
653 This would require, most urgently, a dataset constraining regional horizontal gradients in
654 alkalinity and DIC at near-monthly time scales, as could potentially be developed from
655 algorithms employing satellite data, as well as regional-scale ocean models.

656 Further research into the impacts of climate change on the drivers of the upper ocean carbon
657 cycle, such changes in stratification, precipitation, and biological productivity is needed. The
658 mixed layer carbon budget approach illustrates that a shift in timing or magnitude of the relevant
659 processes over a year could significantly impact observed carbon chemistry, and therefore CO₂
660 source vs. sink behavior of the NPSG.

661 **Acknowledgments**

662 Thank you to Eric Firing for frequent, thorough, and thoughtful support with conceptual and
663 practical challenges. Thanks to the crewmembers and scientists running the Hawaii Ocean Time-
664 series over the last three decades, especially Dan Sadler for the carbonate system samples and
665 measurements. The HOT program is supported by the National Science Foundation (current

666 grant OCE-1756517; AEW, P.I.). The WHOI Hawaii Ocean Timeseries Station (WHOTS) is
667 supported by the National Oceanic and Atmospheric Administration (NOAA) Global Ocean
668 Monitoring and Observing Program through the Cooperative Institute for the North Atlantic
669 Region (CINAR) under Cooperative Agreement NA14OAR4320158. NOAA CPO
670 FundRef number (100007298). Subsurface measurements are supported by NSF as part of the
671 Hawaii Ocean Timeseries (HOT) through grants OCE-752606, 0926766, 1260164 and 1756517.
672 We acknowledge the financial support of our research provided in part by a grant/cooperative
673 agreement from the National Oceanic and Atmospheric Administration, CMAR award #
674 NA21NMF4320043. The views expressed herein are those of the author(s) and do not
675 necessarily reflect the views of NOAA or any of its subagencies. There are no perceived
676 financial or other conflicts of interests for any author. **This is SOEST contribution number ####,**
677 and PMEL contribution number 5449.
678
679

680 **Open Research**

681 Shipboard Hawaii Ocean Time-series bottle and CTD data is available through the HOTDOGS
682 database at <https://hahana.soest.hawaii.edu/hot/hot-dogs/interface.html>. WHOTS and MOSEAN
683 mooring pCO₂, SST and salinity data are available at
684 https://www.nodc.noaa.gov/ocads/oceans/Moorings/WHOTS_158W_23N.html and
685 <https://www.nodc.noaa.gov/ocads/oceans/Moorings/MOSEAN.html>. WHOTS subsurface CTD,
686 ADCP and VMCM datasets can be found at <ftp://mananui.soest.hawaii.edu/pub/hot/whots/>, while
687 surface meteorological data and heat flux can be accessed via
688 <http://uop.whoi.edu/currentprojects/WHOTS/whotsarchive.html>,
689 <http://uop.whoi.edu/ReferenceDataSets/whotsreference.html>, and
690 [http://tds0.ifremer.fr/thredds/catalog/CORIOLIS-OCEANSITES-GDAC-
691 OBS/DATA_GRIDDED/WHOTS/catalog.html?dataset=CORIOLIS-OCEANSITES-GDAC-
692 OBS/DATA_GRIDDED/WHOTS/](http://tds0.ifremer.fr/thredds/catalog/CORIOLIS-OCEANSITES-GDAC-OBS/DATA_GRIDDED/WHOTS/catalog.html?dataset=CORIOLIS-OCEANSITES-GDAC-OBS/DATA_GRIDDED/WHOTS/). Wind stress data is available at
693 http://apdrc.soest.hawaii.edu/erddap/griddap/hawaii_soest_a6ab_91f7_b38f.html. Satellite SST used
694 in the heat budget can be accessed at
695 [http://apdrc.soest.hawaii.edu/thredds/dodsC/las/oisst_avhrrv20/data_apdrc.soest.hawaii.edu_dods
696 public_data_NOAA_SST_OISST_AVHRR_daily_v2.0.jnl](http://apdrc.soest.hawaii.edu/thredds/dodsC/las/oisst_avhrrv20/data_apdrc.soest.hawaii.edu_dods_public_data_NOAA_SST_OISST_AVHRR_daily_v2.0.jnl).

697 **References**

- 698 Anderson, L., and Sarmiento, J. (1994). Redfield ratios of remineralization determined by
699 nutrient data analysis. *Global Biogeochemical Cycles*, 8(1), 65–80.
700
- 701 Ascani, F., Richards, K. J., Firing, E., Grant, S., Johnson, K. S., Jia, Y., Lukas, R., & Karl, D. M.
702 (2013). Physical and biological controls of nitrate concentrations in the upper
703 subtropical North Pacific Ocean. *Deep Sea Research Part II: Topical Studies in
704 Oceanography*, 93, 119-134.
705
- 706 Barone, B., Coenen, A.R., Beckett, S. J., Mcgillicuddy, D. J. Jr., Weitz, J. S., & Karl, D.M., (2019).
707 The ecological and biogeochemical state of the North Pacific Subtropical Gyre is linked
708 to sea surface height. *Journal of Marine Research*, 77(2), 215-245.
709
- 710 Benitez-Nelson, C., Buesseler, K. O., Karl, D. M., & Andrews, J. (2001). A time-series study of

- 711 particulate matter export in the North Pacific Subtropical Gyre based on ^{234}Th : ^{238}U
712 disequilibrium. *Deep Sea Research Part I: Oceanographic Research Papers*, 48(12), 2595-
713 2611.
- 714
- 715 Bittig, H., Steinhoff, T., Claustre, H., Fiedler, B., Williams, N., Sauzède, R., Kötzinger, A., &
716 Gattuso,
717 J., (2018). Nutrient concentrations from T, S, and O₂ data using Bayesian neural
718 networks. *Frontiers in Marine Science*, 5, 328.
- 719
- 720 Böttjer, D., Dore, J.E., Karl, D.M., Letelier, R.M., Mahaffey, C., Wilson, S.T., Zehr, J., Church, M.J.,
721 (2017). Temporal variability of dinitrogen fixation and particulate nitrogen export at
722 Station ALOHA. *Limnology and Oceanography*, 62(1), 200–216.
723 <https://doi.org/10.1002/lno.10386>
- 724
- 725 Boeuf, D., Edwards, B. R., Eppley, J. M., Hu, S. K., Poff, K. E., Romano, A. E., Caron, D.A., Karl,
726 D.M.,
727 & DeLong, E. F. (2019). Biological composition and microbial dynamics of sinking
728 particulate organic matter at abyssal depths in the oligotrophic open ocean. *Proceedings*
729 *of the National Academy of Sciences*, 116(24), 11824-11832.
- 730
- 731 Boyd, P.E., Claustre, H., Levy, M., Siegel, D.A., & Weber, T., (2019). Multi-faceted particle pumps
732 drive carbon sequestration in the ocean. *Nature*, 568, 327-335.
- 733
- 734 Brix, H., Gruber, N., Karl, D., & Bates, N., (2006). On the relationships between primary, net
735 community, and export production in subtropical gyres. *Deep-Sea Research II*, 53, 698-
736 717.
- 737
- 738 Brix, H., Gruber, N., & Keeling, C.D., (2004). Interannual variability of the upper ocean carbon
739 cycle at station ALOHA near Hawaii. *Global Biogeochemical Cycles*, 18, GB4019.
- 740
- 741 Broullón, D., Pérez, F., Velo, A., Hoppema, M., Olsen, A., Takahashi, T., Key, R., Tanhua, T.,
742 González-Dávila, M., Jeansson, E., Kozyr, A. & van Heuven, S., (2019). A global monthly
743 climatology of total alkalinity: A neural network approach. *Earth System Science Data*,
744 11, 1109-1127.
- 745
- 746 Broullón, D., Pérez, F. F., Velo, A., Hoppema, M., Olsen, A., Takahashi, T., Key, R., Tanhua, T.,
747 Santana-Casiano, J. M., & Kozyr, A. (2020). A global monthly climatology of oceanic total
748 dissolved inorganic carbon: a neural network approach. *Earth System Science Data*,
749 12(3), 1725-1743.
- 750
- 751 Carter, B. R., Feely, R. A., Williams, N. L., Dickson, A. G., Fong, M. B., & Takeshita, Y.
752 (2018). Updated methods for global locally interpolated estimation of alkalinity, pH, and
753 nitrate. *Limnology and Oceanography: Methods*, 16(2), 119-131.
- 754

- 755 Church, M.J., Lomas, M.W., & Muller-Karger, F., (2013). Sea change: Charting the course for
756 biogeochemical ocean time-series research in a new millennium. *Deep-Sea Research II*,
757 93, 2-15.
- 758
- 759 Claustré, H., Legendre, L., Boyd, P., & Levy, M. (2021). The oceans' biological carbon pumps:
760 Framework for a research observational community approach. *Frontiers in Marine*
761 *Science*, 8, 780052.
- 762
- 763 Cortés, M.Y., Bollmann, J., & Thierstein, H.R., (2001). Coccolithophore ecology at the HOT
764 station ALOHA, Hawaii. *Deep-Sea Research II*, 48, 1957-1981.
- 765
- 766 Cronin, M. F., Pelland, N. A., Emerson, S. R., & Crawford, W. R. (2015). Estimating diffusivity
767 from the mixed layer heat and salt balances in the North Pacific. *Journal of Geophysical*
768 *Research: Oceans*, 120(11), 7346-7362.
- 769 De Boyer Montégut, C., Madec, G., Fischer, A.S., Lazar, A., & Iudicone, D., (2004).
770 Mixed layer depth over the global ocean: An examination of profile data and a profile-
771 based climatology. *Journal for Geophysical Research - Oceans* 109(C12), C12003. doi:
772 10.1029/2004JC002378
- 773
- 774 Denman, K. L., & Gargett, A. E. (1983). Time and space scales of vertical mixing and advection of
775 phytoplankton in the upper ocean. *Limnology and Oceanography*, 28(5), 801-815.
- 776
- 777 Dickson, A.G., (1990). Standard Potential of the Reaction: $\text{AgCl(s)} + 1/2\text{H}_2(\text{g}) = \text{Ag(s)} + \text{HCl(aq)}$,
778 and the Standard Acidity Constant of the Ion HSO_4^- in Synthetic Seawater from 273.15
779 to 318.15 K. *Journal of Chemical Thermodynamics*, 22(2), 113-127. doi:10.1016/0021-
780 9614(90)90074-Z
- 781
- 782 Dickson, A. G., and Riley, J. P. (1979). The estimation of acid dissociation constants in sea-water
783 media from potentiometric titrations with strong base. II. The dissociation of phosphoric
784 acid. *Marine Chemistry* 7, 101–109. [doi:10.1016/0304-4203\(79\)90002-1](https://doi.org/10.1016/0304-4203(79)90002-1).
- 785
- 786 Dong, S., Berelson, W., Rollins, N., Subhas, A., Naviaux, J., Celestian, A., Liu, X., Turaga, N.,
787 Kemnitz, N., Byrne, R., & Adkins, J., (2019). Aragonite dissolution kinetics and
788 calcite/aragonite ratios in sinking and suspended particles in the North Pacific. *Earth and*
789 *Planetary Science Letters*, 515, 1-12.
- 790
- 791 Dore, J., Church, M., Karl, D., Sadler, D., & Letelier, R. (2014). Paired windward and leeward
792 biogeochemical time series reveal consistent surface ocean CO₂ trends across the
793 Hawaiian Ridge. *Geophysical Research Letters*, 41, 6459-6467.
- 794
- 795 Dore, J. E., Lukas, R., Sadler, D.W., Church, M.J., & Karl, D.M., (2009). Physical and
796 biogeochemical

- 797 modulation of ocean acidification in the central North Pacific. *PNAS*, 106(30), 12235-
798 12240.
- 799
- 800 Dore, J., Lukas, R., Sadler, D., & Karl, D., (2003). Climate-driven changes to atmospheric CO₂ sink
801 in the subtropical North Pacific Ocean. *Nature*, 424, 754-757.
- 802
- 803 Duarte, C. M., Regaudie-de-Gioux, A., Arrieta, J. M., Delgado-Huertas, A., & Agustí, S. (2013).
804 The oligotrophic ocean is heterotrophic. *Annual Review of Marine Science*, 5, 551–569.
805 <https://doi.org/10.1146/annurev-marine-121211-172337>
- 806
- 807 Ducklow, H. W., & Doney, S. C. (2013). What is the metabolic state of the oligotrophic ocean? A
808 debate. *Annual Review of Marine Science*, 5, 525–533. [https://doi.org/10.1146/annurev-](https://doi.org/10.1146/annurev-marine-121211-172331)
809 [marine-121211-172331](https://doi.org/10.1146/annurev-marine-121211-172331)
- 810
- 811 Emerson, S. (2014), Annual net community production and the biological carbon flux in the
812 ocean, *Global Biogeochem. Cycles*, 28, 14– 28, doi:[10.1002/2013GB004680](https://doi.org/10.1002/2013GB004680).
- 813
- 814 Emerson, S., Quay, P. D., Karl, D. M., Winn, C., Tupas, L., & Landry, M. (1997). Experimental
815 determination of the organic carbon flux from open-ocean surface waters. *Nature*, 389,
816 951–954. <https://doi.org/10.1038/40111>
- 817 Emerson, S., Quay, P. D., Stump, C., Wilbur, D., & Schudlich, R. (1995). Chemical tracers of
818 productivity and respiration in the subtropical Pacific Ocean. *Journal of Geophysical*
819 *Research*, 100, 873–887. <https://doi.org/10.1029/95jc01333>
- 820
- 821 Emerson, S., Stump, C., & Nicholson, D. P. (2008). Net biological oxygen production in the
822 ocean: Remote in situ measurements of O₂ and N₂ in surface waters. *Global*
823 *Biogeochemical Cycles*, 22, GB3023. <https://doi.org/10.1029/2007GB003095>
- 824
- 825 Fassbender, A.J., Sabine, C.L., & Cronin, M.F., (2016). Net community production and
826 calcification from 7 years of NOAA Station Papa Mooring measurements. *Global*
827 *Biogeochemical Cycles*, 30, 250-257.
- 828
- 829 Fassbender, A.J., Sabine, C.L., Cronin, M.F., & Sutton, A.J., (2017). Mixed-layer carbon cycling at
830 the Kuroshio Extension Observatory. *Global Biogeochemical Cycles*, 31, 272-288.
- 831
- 832 Fernández-Castro, B., Mouriño-Carballido, B., Benítez-Barrios, V. M., Chouciño, P., Fraile-Nuez,
833 E., Graña, R., Piedeleu, M., & Rodríguez-Santana, A. (2014). Microstructure turbulence
834 and diffusivity parameterization in the tropical and subtropical Atlantic, Pacific and
835 Indian Oceans during the Malaspina 2010 expedition. *Deep Sea Research Part I:*
836 *Oceanographic Research Papers*, 94, 15-30.
- 837
- 838 Ferrón, S., Barone, B., Church, M.J., White, A.E., & Karl, D.M., (2021). Euphotic zone metabolism
839 in the North Pacific Subtropical Gyre based on oxygen dynamics. *Global Biogeochemical*
840 *Cycles*, 35, e2020GB006744. doi: 10.1029/2020GB006744

- 841
842 Firing, E., (1996). Currents observed north of Oahu during the first five years of HOT. *Deep Sea*
843 *Research II*, 43(2-3), 281-303.
- 844
845 Follett, C. L., Dutkiewicz, S., Karl, D. M., Inomura, K., & Follows, M. J. (2018). Seasonal resource
846 conditions favor a summertime increase in North Pacific diatom–diazotroph
847 associations. *The ISME journal*, 12(6), 1543-1557.
- 848
849 Gruber, N., & Sarmiento, J. L. (1997). Global patterns of marine nitrogen fixation and
850 denitrification. *Global biogeochemical cycles*, 11(2), 235-266.
- 851
852 Hamme, R. C., & Emerson, S. (2004). The solubility of neon, nitrogen and argon in distilled
853 water
854 and seawater. *Deep-Sea Research Part I: Oceanographic Research Papers*, 51, 1517–
855 1528. <https://doi.org/10.1016/j.dsr.2004.06.009>
- 856
857 Hastenrath, S., & Merle, J. (1987). Annual cycle of subsurface thermal structure in the tropical
858 Atlantic Ocean. *Journal of Physical Oceanography*, 17(9), 1518-1538.
- 859
860 Ho, D. T., Law, C., Smith, M., Schlosser, P., Harvey, M., & Hill, P., (2006). Measurements of air-
861 sea gas exchange at high wind speeds in the Southern Ocean: Implications for global
862 parameterizations. *Geophysical Research Letters*, 33, L16611.
- 863
864 Humphreys, M. P., Lewis, E. R., Sharp, J. D., and Pierrot, D. (2022a). PyCO2SYS v1.8: marine
865 carbonate system calculations in Python. *Geoscientific Model Development* 15, 15-43.
866 doi:10.5194/gmd-15-15-2022.
- 867
868 Humphreys, M. P., Schiller, A. J., Sandborn, D. E., Gregor, L., Pierrot, D., van Heuven, S. M. A. C.,
869 Lewis, E. R., and Wallace, D. W. R. (2022b). PyCO2SYS: marine carbonate system
870 calculations in Python. *Zenodo*. [doi:10.5281/zenodo.3744275](https://doi.org/10.5281/zenodo.3744275).
- 871
872 Johnson, G.C., (2001). The Pacific Ocean subtropical cell surface limb. *Geophysical Research*
873 *Letters*, 28(9), 1771-1774.
- 874
875 Kara, A. B., Rochford, P. A., & Hurlburt, H. E. (2000). An optimal definition for ocean mixed layer
876 depth. *Journal of Geophysical Research: Oceans*, 105(C7), 16803-16821.
- 877
878 Karl, D. M. (1999). A Sea of Change: Biogeochemical Variability in the North Pacific
879 Subtropical Gyre. *Ecosystems*, 2(3), 181–214.
- 880
881 Karl, D. M., Christian, J. R., Dore, J. E., Hebel, D. V., Letelier, R. M., Tupas, L. M., & Winn, C. D.,
882 (1996). Seasonal and interannual variability in primary production and particle flux at
883 Station ALOHA. *Deep Sea Research II*, 43(2-3), 539-568.
- 884

- 885 Karl, D., & Church, M. (2017). Ecosystem structure and dynamics in the North Pacific
886 Subtropical Gyre: New views of an old ocean. *Ecosystems*, 20, 433-457.
887
- 888 Karl, D., & Church, M. (2018). Station ALOHA: A gathering place for discovery, education, and
889 scientific collaboration. *Limnology and Oceanography Bulletin*.
- 890 Karl, D.M., Letelier, R.M., Bidigare, R.R., Björkman, K.M., Church, M.J., Dore, J.E., & White, A.E.,
891 (2021). Seasonal-to-decadal scale variability in primary production and particulate
892 matter export at Station ALOHA. *Progress in Oceanography*. doi:
893 <https://doi.org/10.1016/j.pocean.2021.102563>
- 894 Karl, D. M., & Lukas, R. (1996). The Hawaii Ocean Time-series (HOT) program: Background,
895 rationale and field implementation. *Deep Sea Research Part II: Topical Studies in*
896 *Oceanography*, 43(2-3), 129–156. doi:10.1016/0967-0645(96)00005-7
897
- 898 Keeling, C.D., Brix, H., & Gruber, N., (2004). Seasonal and long-term dynamics of the upper
899 ocean carbon cycle at Station ALOHA near Hawaii. *Global Biogeochemical Cycles*, 18,
900 GB4006.
901
- 902 Letelier, R.M., Karl, D.M., Abbott, M.R., Flament, P., Freilich, M., Lukas, R., & Strub, T., (2000).
903 Role of late winter mesoscale events in the biogeochemical variability of the upper
904 water column of the North Pacific Subtropical Gyre. *Journal of Geophysical Research*,
905 105(C12), 287723-28739.
906
- 907 Lee, K. (2001). Global net community production estimated from the annual cycle of surface
908 water total dissolved inorganic carbon. *Limnology & Oceanography*, 46, 1287–1297.
909 <https://doi.org/10.4319/lo.2001.46.6.1287>
910
- 911 Levitus, S. (1982). *Climatological atlas of the world ocean* (Vol. 13). US Department of
912 Commerce, National Oceanic and Atmospheric Administration.
913
- 914 Liu, W. T., Katsaros, K. B., & Businger, J. A. (1979). Bulk parameterization of air-sea exchanges of
915 heat and water vapor including the molecular constraints at the interface. *Journal of the*
916 *Atmospheric Sciences*, 36(9), 1722-1735.
917
- 918 Lueker, T. J., Dickson, A. G., & Keeling, C. D. (2000). Ocean pCO₂ calculated from dissolved
919 inorganic carbon, alkalinity, and equations for K₁ and K₂: validation based on laboratory
920 measurements of CO₂ in gas and seawater at equilibrium. *Marine Chemistry*, 70(1-3),
921 105-119.
922
- 923 Lukas, R., & Santiago-Mandujano, F. (2008). Interannual to interdecadal salinity variations
924 observed near Hawaii: Local and remote forcing by surface freshwater fluxes.
925 *Oceanography*, 21(1), 46-55.

- 926
927 McLaughlin, K., S.B. Weisberg, A.G. Dickson, G.E. Hofmann, J.A. Newton, D. Aseltine-Neilson, A.
928 Barton, S. Cudd, R.A. Feely, I.W. Jefferds, and others, (2015). Core principles of the
929 California Current Acidification Network: Linking chemistry, physics, and ecological
930 effects. *Oceanography* 28(2), 160–169.
931
- 932 Monteagudo, M. M. (2016). *Planktonic foraminiferal faunal study and Mg/Ca-temperature*
933 *calibration at the Hawaii Ocean Time-Series*. University of California, Santa Barbara.
934
- 935 Neuer, S., Davenport, R., Freudenthal, T., Wefer, G., Llinás, O., Rueda, M.-J., Steinberg, D. K.,
936 & Karl, D. M., (2002). Differences in the biological carbon pump at three subtropical
937 ocean sites, *Geophys. Res. Lett.*, 29(18), 1885, doi:[10.1029/2002GL015393](https://doi.org/10.1029/2002GL015393).
938
- 939 Nickford, S., J.B. Palter, K. Donohue, A.J. Fassbender, A.R. Gray, J. Long, A.J. Sutton, N.R. Bates,
940 and Y. Takeshita (2022). Autonomous Wintertime Observations of Air-Sea Exchange in
941 the Gulf Stream Reveal a Perfect Storm for Ocean CO₂ Uptake. *Geophysical Research*
942 *Letters*, 49(5), e2021GL096805, <https://doi.org/10.1029/2021GL096805>.
943
- 944 Nicholson, S.-A., D.B. Whitt, I. Fer, M.D. du Plessis, A.D. Lebéhot, S. Swart, A.J. Sutton, and
945 P.M.S. Monteiro. 2022. Storms drive outgassing of CO₂ in the subpolar Southern Ocean.
946 *Nature Communications* 13(1), 158, [10.1038/s41467-021-27780-w](https://doi.org/10.1038/s41467-021-27780-w).
947
- 948 Nightingale, P. D., Malin, G., Law, C. S., Watson, A. J., Liss, P. S., Liddicoat, M. I., Boutin, J., &
949 Upstill-Goddard, R. C. (2000). In situ evaluation of air-sea gas exchange
950 parameterizations using novel conservative and volatile tracers. *Global Biogeochemical*
951 *Cycles*, 14(1), 373-387.
952
- 953 Orr, J. C., Epitalon, J. M., Dickson, A. G., & Gattuso, J. P. (2018). Routine uncertainty propagation
954 for the marine carbon dioxide system. *Marine Chemistry*, 207, 84-107.
955
- 956 Quay, P. D., Peacock, C., Björkman, K., & Karl, D. M. (2010). Measuring primary production rates
957 in the ocean: Enigmatic results between incubation and non - incubation methods at
958 Station ALOHA. *Global Biogeochemical Cycles*, 24, GB3014.
959 <https://doi.org/10.1029/2009GB003665>
960
- 961 Quay, P. D., Stutsman, J., Feely, R. A., & Juranek, L. W. (2009). Net community production rates
962 across the subtropical and equatorial Pacific Ocean estimated from air-sea $\delta^{13}\text{C}$
963 disequilibrium. *Global Biogeochemical Cycles*, 23, GB2006.
964 <https://doi.org/10.1029/2008GB003193>
965
- 966 Quay, P., & Stutsman, J., (2003). Surface layer carbon budget for the subtropical N. Pacific: $\delta^{13}\text{C}$
967 constraints at Station ALOHA. *Deep-Sea Research Part I – Oceanographic Research*
968 *Papers*, 50(9), 1045-1061.
969

- 970 Riser, S. C., & Johnson, K. S. (2008). Net production of oxygen in the subtropical ocean. *Nature*,
 971 451, 323–325. <https://doi.org/10.1038/nature06441>
 972
- 973 Sabine, C.L., Maenner Jones, S., Bott, R., Sutton, A.J., (2012). High-resolution ocean and
 974 atmosphere pCO₂ time-series measurements from mooring MOSEAN_158W_23N (NCEI
 975 Accession 0100073). [complete dataset]. NOAA National Centers for Environmental
 976 Information. Dataset. https://doi.org/10.3334/cdiac/otg.tsm_mosean. Accessed
 977 11/15/2022.
 978
- 979 Sabine, C., & Mackenzie, F., (1995). Bank-derived carbonate sediment transport and dissolution
 980 in the Hawaiian archipelago. *Aquatic Geochemistry*, 1, 189-230.
 981
- 982 Sabine, C. L., Mackenzie, F. T., Winn, C., & Karl, D. M. (1995). Geochemistry of carbon dioxide in
 983 seawater at the Hawaii Ocean Time series station, ALOHA. *Global Biogeochemical*
 984 *Cycles*, 9(4), 637-651.
 985
- 986 Santiago-Mandujano, F., Lukas, R., Murphy, D. J., & Larson, N. G. (2016). MicroCAT/SeaCAT
 987 Sensor Calibration and Data Quality Control: Lessons Learned from 10 Years of WHOI-
 988 Hawaii Ocean Time-Series Site (WHOTS) Mooring Deployments. *American Geophysical*
 989 *Union*, 2016, OD14C-2432.
 990
- 991 Sonnerup, R. E., Mecking, S., & Bullister, J. L. (2013). Transit time distributions and oxygen
 992 utilization rates in the Northeast Pacific Ocean from chlorofluorocarbons and sulfur
 993 hexafluoride. *Deep-Sea Research Part I: Oceanographic Research Papers*, 72, 61–71.
 994 <https://doi.org/10.1016/j.dsr.2012.10.013>
 995
- 996 Sonnerup, R. E., Quay, P. D., & Bullister, J. L. (1999). Thermocline ventilation and oxygen
 997 utilization rates in the subtropical North Pa- cific based on CFC distributions during
 998 WOCE. *Deep-Sea Research Part I: Oceanographic Research Papers*, 45, 777–805.
 999 [https://doi.org/10.1016/S0967-0637\(98\)00092-2](https://doi.org/10.1016/S0967-0637(98)00092-2)
 1000
- 1001 Sprintall, J., & Tomczak, M. (1992). Evidence of the barrier layer in the surface layer of the
 1002 tropics. *Journal of Geophysical Research: Oceans*, 97(C5), 7305-7316.
 1003
- 1004 Steinberg, D. K., Cope, J. S., Wilson, S. E., & Kobari, T., (2008). A comparison of mesopelagic
 1005 mesozooplankton community structure in the subtropical and subarctic North Pacific
 1006 Ocean. *Deep Sea Research Part II: Topical Studies in Oceanography*, 55(14-15), 1615-
 1007 1635.
 1008
- 1009 Sulpis, O., Lauvset, S. K., and Hagens, M. (2020). Current estimates of K_1^* and K_2^* appear
 1010 inconsistent with measured CO₂ system parameters in cold oceanic regions. *Ocean*
 1011 *Science* 16(4), 847–862. [doi:10.5194/os-2020-19](https://doi.org/10.5194/os-2020-19).
 1012
- 1013 Sutton, A. J., Sabine, C.L., Dietrich, C., Maenner Jones, S., Musielewicz, S., Bott, R., & Osborne,

- 1014 J., (2012). High-resolution ocean and atmosphere pCO₂ time-series measurements from
 1015 mooring WHOTS_158W_23N in the North Pacific Ocean (NCEI Accession 0100080).
 1016 [indicate subset used]. NOAA National Centers for Environmental Information. Dataset.
 1017 https://doi.org/10.3334/cdiac/otg.tsm_whots. Accessed [11/15/2022].
 1018
- 1019 Sutton, A.J., C.L. Sabine, R.A. Feely, W.J. Cai, M.F. Cronin, M.J. McPhaden, J.M. Morell, J.A.
 1020 Newton, J.H. Noh, S.R. Ólafsdóttir, and others, (2016). Using present-day observations
 1021 to detect when anthropogenic change forces surface ocean carbonate chemistry outside
 1022 preindustrial bounds. *Biogeosciences* 13(17), 5065-5083, 10.5194/bg-13-5065-2016.
 1023
- 1024 Sutton, A. J., Sabine, C. L., Maenner-Jones, S., Lawrence-Slavas, N., Meinig, C., Feely, R. A.,
 1025 Mathis, J. T., Musielewicz, S., Bott, R., McLain, P. D., Fought, H. J., & Kozyr, A. (2014). A
 1026 high-frequency atmospheric and seawater pCO₂ data set from 14 open-ocean sites using
 1027 a moored autonomous system. *Earth System Science Data*, 6(2), 353-366.
 1028
- 1029 Tomczak, M., & Godfrey, J.S., (2003). *Regional Oceanography: An Introduction*, 2nd ed., 390 pp.,
 1030 Daya, Delhi, India.
 1031
- 1032 Uppström, L. R. (1974). The boron/chlorinity ratio of deep-sea water from the Pacific Ocean.
 1033 *Deep-Sea Research* 21, 161–162. [doi:10.1016/0011-7471\(74\)90074-6](https://doi.org/10.1016/0011-7471(74)90074-6).
 1034
- 1035 Venrick, E. L., (1993). Phytoplankton seasonality in the Central North Pacific: The endless
 1036 summer
 1037 reconsidered. *Limnology and Oceanography*, 28(6), 1135-1149.
 1038
- 1039 Wanninkhof, R. (1992), Relationship between wind speed and gas exchange over the ocean.
 1040 *Journal of Geophysical Research*, 97(C5), 7373–7382.
 1041
- 1042 Weiss, R. (1974), Carbon dioxide in water and seawater: The solubility of a non-ideal gas,
 1043 *Marine Chemistry*, 2(3), 203–215.
 1044
- 1045 Weller, R.A. & David, R.E., (1980). A vector measuring current meter. *Deep-Sea Research*, 27A,
 1046 565-582.
 1047
- 1048 Williams, P. J. L. B., Quay, P. D., Westberry, T. K., & Behrenfeld, M. J. (2013). The oligotrophic
 1049 ocean is autotrophic. *Annual Review of Marine Science*, 5, 535–549.
 1050 <https://doi.org/10.1146/annurev-marine-121211-172335>
 1051
- 1052 Wilson, S., Barone, B., Ascani, F., Bidgare, R.R., Church, M.J., del Valle, D.A., Dyhrman, S.T.,
 1053 Ferrón, S., Fitzsimmons, J.N., Juranek, L.W., Kolber, Z.S., Letelier, R.M., Martínez-García,
 1054 S., Nicholson, D.P., Richards, K.J., Rii, Y.M., Rouco, M., Viviani, D.A., White, A.E., Zehr,
 1055 J.P., Karl, D.M., (2015). Short-term variability in euphotic zone biogeochemistry and
 1056 primary productivity at Station ALOHA: A case study of summer 2012. *Global*
 1057 *Biogeochemical Cycles*, 29, 1145-1164.

1058

1059 Winn, C. D., Mackenzie, F. T, Carrillo, C. J., Sabine, C. L., & Karl, D. M., (1994). Air- sea carbon
1060 dioxide exchange in the North Pacific Subtropical Gyre: Implications for the global
1061 carbon budget. *Global Biogeochemical Cycles*, 8(2), 157-163.

1062

1063 Winn, C. D., Li, Y.H., Mackenzie, F. T., & Karl, D. M., (1998). Rising surface ocean dissolved
1064 inorganic carbon at the Hawaii Ocean Time-series site. *Marine Chemistry*, 60, 33-47.

1065

1066 Yang, B., Emerson, S., & Bushinsky, S. M. (2017). Annual net community production in the
1067 subtropical Pacific Ocean from in situ oxygen measurements on profiling floats. *Global*
1068 *Biogeochemical Cycles*, 31, 728–744. <https://doi.org/10.1002/2016GB005545>

1069

1070 Zhurbas, V., & Oh, I.S., (2004). Drifter-derived maps of lateral diffusivity in the Pacific and
1071 Atlantic Oceans in relation to surface circulation patterns. *Journal of Geophysical*
1072 *Research*, 109, C05015.